B cell-specific conditional expression of Myd88(p.L252P) leads to the development of diffuse large B cell lymphoma in mice

Knittel, G. and Liedgens, P. and Korovkina, D. and Seeger, J.M. and Al-Baldawi, Y. and Al-Maarri, M. and Fritz, C. and Vlantis, K. and Bezhanova, S. and Scheel, A.H. and Wolz, O.O. and Reimann, M. and Moeller, P. and Lopez, C. and Schlesner, M. and Lohneis, P. and Weber, A.N.R. and Truemper, L. and Staudt, L.M. and Ortmann, M. and Pasparakis, M. and Siebert, R. and Schmitt, C.A. and Klatt, A.R. and Wunderlich, F.T. and Schaefer, S.C. and Persigehl, T. and Montesinos-Rongen, M. and Odenthal, M. and Buettner, R. and Frenzel, L.P. and Kashkar, H. and Reinhardt, H.C.

This is a copy of the final article, which was first published online on 05 APRIL 2016 and in final edited form in:

Blood
2016 JUN 02 ; 127(22): 2732-2741
doi: 10.1182/blood-2015-11-684183

Publisher: The American Society of Hematology

LYMPHOID NEOPLASIA

B-cell–specific conditional expression of *Myd88*$^{p.L252P}$ leads to the development of diffuse large B-cell lymphoma in mice

Gero Knittel,[1,2,*] Paul Liedgens,[1,2,*] Darya Korovkina,[1,2,*] Jens M. Seeger,[2,3,*] Yussor Al-Baldawi,[4] Mona Al-Maarri,[5] Christian Fritz,[1,2] Katerina Vlantis,[2] Svetlana Bezhanova,[6,7] Andreas H. Scheel,[6] Olaf-Oliver Wolz,[8] Maurice Reimann,[9] Peter Möller,[10] Cristina López,[11] Matthias Schlesner,[12] Philipp Lohneis,[13] Alexander N. R. Weber,[8] Lorenz Trümper,[14] German International Cancer Genome Consortium Molecular Mechanisms in Malignant Lymphoma by Sequencing Project Consortium, Louis M. Staudt,[15] Monika Ortmann,[6] Manolis Pasparakis,[2] Reiner Siebert,[11] Clemens A. Schmitt,[9,16] Andreas R. Klatt,[17] F. Thomas Wunderlich,[5] Stephan C. Schäfer,[6] Thorsten Persigehl,[4] Manuel Montesinos-Rongen,[18] Margarete Odenthal,[6,19] Reinhard Büttner,[6,19,20] Lukas P. Frenzel,[1,2,19,†] Hamid Kashkar,[2,3,20,†] and H. Christian Reinhardt[1,2,19,20,†]

[1]Department I of Internal Medicine, University Hospital of Cologne, Cologne, Germany; [2]Cologne Excellence Cluster on Cellular Stress Response in Aging-Associated Diseases, University of Cologne, Cologne, Germany; [3]Institute for Microbiology and Hygiene, and [4]Department of Radiology, Medical Faculty, University Hospital of Cologne, Cologne, Germany; [5]Max Planck Institute for Metabolism Research, Cologne, Germany; [6]Institute of Pathology, University Hospital of Cologne, Cologne, Germany; [7]N.N. Blokhin Russian Cancer Research Center, Moscow, Russia; [8]Interfaculty Institute for Cell Biology, Department of Immunology, University of Tübingen, Tübingen, Germany; [9]Department of Hematology/Oncology, Charité-University Medical Center, Berlin, Germany; [10]Institute of Pathology, Medical Faculty of Ulm University, Ulm, Germany; [11]Institute for Human Genetics, Christian-Albrechts-University Kiel and University Hospital Schleswig-Holstein, Kiel, Germany; [12]Department of Theoretical Bioinformatics, German Cancer Research Center, Heidelberg, Germany; [13]Department of Pathology, Charité-University Medical Center, Berlin, Germany; [14]Department of Hematology and Oncology, Georg-August University, Goettingen, Germany; [15]Metabolism Branch, Center for Cancer Research, National Cancer Institute, National Institutes of Health, Bethesda, MD; [16]Max Delbrück Center for Molecular Medicine in the Helmholtz Association, Berlin, Germany; [17]Institute for Clinical Chemistry, [18]Institute of Neuropathology, and [19]Center of Integrated Oncology, University Hospital of Cologne, Cologne, Germany; and [20]Center of Molecular Medicine, University of Cologne, Cologne, Germany

Key Points

- B-cell–specific expression of *Myd88*$^{p.L252P}$ leads to the development of DLBCL in mice.
- The *Myd88*$^{p.L252P}$ mutation cooperates with *BCL2* amplifications in ABC-DLBCL lymphomagenesis in vivo.

The adaptor protein MYD88 is critical for relaying activation of Toll-like receptor signaling to NF-κB activation. *MYD88* mutations, particularly the p.L265P mutation, have been described in numerous distinct B-cell malignancies, including diffuse large B-cell lymphoma (DLBCL). Twenty-nine percent of activated B-cell–type DLBCL (ABC-DLBCL), which is characterized by constitutive activation of the NF-κB pathway, carry the p.L265P mutation. In addition, ABC-DLBCL frequently displays focal copy number gains affecting *BCL2*. Here, we generated a novel mouse model in which Cre-mediated recombination, specifically in B cells, leads to the conditional expression of *Myd88*$^{p.L252P}$ (the orthologous position of the human *MYD88*$^{p.L265P}$ mutation) from the endogenous locus. These mice develop a lymphoproliferative disease and occasional transformation into clonal lymphomas. The clonal disease displays the morphologic and immunophenotypical characteristics of ABC-DLBCL. Lymphomagenesis can be accelerated by crossing in a further novel allele, which mediates conditional overexpression of *BCL2*. Cross-validation experiments in human DLBCL samples revealed that both *MYD88* and *CD79B* mutations are substantially enriched in ABC-DLBCL compared with germinal center B-cell DLBCL. Furthermore, analyses of human DLBCL genome sequencing data confirmed that *BCL2* amplifications frequently co-occurred with *MYD88* mutations, further validating our approach. Finally, in silico experiments revealed that *MYD88*-mutant ABC-DLBCL cells in particular display an actionable addiction to BCL2. Altogether, we generated a novel autochthonous mouse model of ABC-DLBCL that could be used as a preclinical platform for the development and validation of novel therapeutic approaches for the treatment of ABC-DLBCL. (*Blood*. 2016;127(22):2732-2741)

Introduction

Toll-like receptors (TLRs) belong to a class of pattern-recognition receptors.[1] Ten distinct human TLRs have been described.[1] Except for TLR3, all TLRs require the adaptor protein MYD88 to initiate downstream signaling.[1,2] Upon TLR activation, MYD88 is recruited to the Toll/interleukin-1 receptor (TIR) domain of the activated TLR via its own TIR domain.[3] MYD88 recruits IRAK1, -2, and -4 to ultimately

Submitted November 30, 2015; accepted March 30, 2016. Prepublished online as *Blood* First Edition paper, April 5, 2016; DOI 10.1182/blood-2015-11-684183.

*G.K., P.L., D.K., and J.M.S. contributed equally to this study.

†L.P.F., H.K., and H.C.R. contributed equally to this study.

The online version of this article contains a data supplement.

There is an Inside *Blood* Commentary on this article in this issue.

The publication costs of this article were defrayed in part by page charge payment. Therefore, and solely to indicate this fact, this article is hereby marked "advertisement" in accordance with 18 USC section 1734.

form the myddosome.[4] IRAK4-mediated phosphorylation of IRAK1 and IRAK2 promotes TRAF6 recruitment,[5] which subsequently ubiquitylates and activates TAK1,[6] leading to NF-κB activation.[2]

Inappropriate TLR signaling through somatic *MYD88* mutations has been described in numerous hematologic malignancies, such as chronic lymphocytic leukemia (CLL),[7] Waldenström macroglobulinemia,[8] and diffuse large B-cell lymphoma (DLBCL).[9] Specifically, 29% of activated B-cell–type DLBCLs (ABC-DLBCLs), which typically display constitutive NF-κB activation, carry the p.L265P mutation (position according to the protein accession NP_002459) in the hydrophobic core of the MYD88 TIR domain.[9] ABC-DLBCL was shown to display *MYD88*$^{p.L265P}$-dependent NF-κB activation and STAT3 phosphorylation.[9] The *MYD88*$^{p.L265P}$ mutation is exceedingly rare in non-ABC-DLBCLs, such as germinal center B-cell (GCB) and primary mediastinal B-cell lymphoma.[9] Moreover, *MYD88*$^{p.L265P}$-mutant ABC-DLBCL appears to be dependent on continued *MYD88*$^{p.L265P}$ expression.[9] Together, these data implicate MYD88-dependent oncogenic NF-κB signaling as an integral contributor to ABC-DLBCL pathogenesis and as a potential therapeutic target. However, despite the clinical relevance of the *MYD88*$^{p.L265P}$ mutation, no autochthonous mouse model that faithfully mimics this critical genomic aberration has yet been generated.

Materials and methods

Experimental mice

B-cell–specific Cre expression was achieved by using *Cd19*^{Cre},[10] *Aid*^{Cre},[11] and *Cd21*^{Cre}[12] deleter mouse strains (The Jackson Laboratory). The targeting vector depicted in Figure 1A was constructed by using standard techniques. The gene targeting strategy was based on the National Center for Biotechnology Information transcript *NM_010851.2* in which exon 1 contains the translation initiation codon. Wild-type (wt) exons 2-6, including the entire 3′ untranslated region were flanked with *LoxP* sites. An additional polyadenylation signal (human growth hormone polyadenylation [hGHpA] signal) has been inserted between the 3′ untranslated region and the distal *LoxP* site to prevent downstream transcription of the mutated exon 5. The size of the *LoxP*-flanked region is 4.7 kb. Exons 2-6, including the splice acceptor site of intron 1, have been duplicated and inserted downstream of the distal *LoxP* site. The p.L252P mutation has been introduced into the duplicated exon 5. Positive selection markers were flanked by *Frt* (neomycin resistance; *Neo*^{R}) and *F3* (puromycin resistance; *Puro*^{R}) sites and inserted into intron 1 and downstream of the hGHpA, respectively. The targeting vector was generated by using BAC clones from the *C57BL/6J* RPCIB-731 BAC library and was transfected into the *C57BL/6N* Tac embryonic stem (ES) cell line. Targeted clones were isolated by using double positive (*Neo*^{R} and *Puro*^{R}) selection, and correct integration was verified by Southern blotting. Upon blastocyst injection, germ line–transmitting transgenic mice were received. The conditional *Myd88*$^{c\text{-}p.L252P}$ allele was obtained after in vivo Flp-mediated removal of the selection markers. This allele expresses the wild-type Myd88 protein, because the presence of the hGHpA cassette downstream of wild-type exon 6 prevents transcription of the mutant exons 2-6. The constitutive *Myd88*$^{p.L252P}$ allele is obtained after in vivo Cre-mediated deletion of wild-type exons 2-6 and hGHpA. This allele expresses the mutant Myd88^{L252P} protein. The remaining recombination sites are located in nonconserved regions of the genome. To generate conditional *BCL2* knockin mice (*Rosa26*$^{LSL.BCL2.IRES.GFP}$), a *Rosa26* locus-targeting vector was used in which CAGS (cytomegalovirus early enhancer/chicken β actin) promoter-driven expression of the transgene (*BCL2*) and downstream expression of an internal ribosomal entry site–driven green fluorescent protein (IRES-GFP, as a reporter for Cre-mediated recombination) is prevented by a *LoxP*-flanked STOP cassette (supplemental Figure 5C, available on the *Blood* Web site). The transgenic mice expressed the transgenes only after Cre-mediated excision of the *LoxP*-flanked STOP cassette. The targeting vector was electroporated into ES cells (BRUCE4), which were screened for correct integration by standard Southern blot methods. Correctly targeted ES cells were used to generate chimeras, which were back-crossed onto a pure *C57BL/6N* background and examined for germ line transmission.

The *Eμ:Myc* model has been described earlier and was used, as previously described.[13] The *Eμ:Tcl1* model of CLL was described earlier.[14] All the experiments that involved the breeding and/or treatment of rodents were approved by the local animal care committee and the relevant authorities (Landesamt für Natur, Umwelt und Verbraucherschutz Nordrhein-Westfalen, AZ: 84-02.04.2014.A146/A083).

Transplantation experiments

Animal protocols based on the *Eμ:Myc* transgenic mouse model as used in this study were approved by the local governmental review board (Landesamt Berlin) and conformed to regulatory standards. Isolation, retroviral infection, transplantation of *Eμ:Myc* transgenic fetal liver cells (ie, hematopoietic stem cells), and subsequent monitoring of the recipient mice regarding lymphoma onset were performed as previously described.[15] Specifically, numerous independently isolated fetal liver cell populations were stably transduced with a murine stem cell virus-based *Myd88*$^{p.L252P\text{-}IRES\text{-}GFP}$ retrovirus or a murine stem cell virus–empty GFP construct as a control before their propagation in recipient mice.

Immunohistochemistry

Formalin-fixed paraffin-embedded (FFPE) murine samples were sliced at 2 to 4 μm. Sections were stained with hematoxylin and eosin (H&E) and antibodies against Ki-67 (Cell Marque), B220 (RA3-6B2BD,), p65 (C-20; Santa Cruz,), Irf4 (M-17; Santa Cruz Biotechnology,), Bcl6 (C-19; Santa Cruz Biotechnology), and Cd138 (553712; BD). Staining intensities were scored by 2 independent observers who used a 4-tier scale. FFPE human samples were sliced at 2 to 4 μm. Sections were stained with H&E and antibodies against CD10 (NCL-L-CD10-270; Novocastra), BCL6 (M7211; Dako), IRF4 (M7259; Dako), BCL2 (M0877; Dako), and CD138 (138M-16; Cell Marque).

Sequence analysis of immunoglobulin genes and cloning of polymerase chain reaction products

RNA was extracted from sections of frozen biopsies with TRI Reagent (Sigma, Taufkirchen, Germany). One microgram of RNA was converted to complementary DNA with QuantiTect Reverse Transcription Kit (Qiagen, Hilden, Germany). Mouse *IgH* rearrangements were analyzed by using previously published methods.[16] Each polymerase chain reaction (PCR) was analyzed on a Qiaxcel Advanced Instrument (Qiagen) by using ScreenGel Software v1.2. Direct sequencing was performed with the ABI Prism Dye Terminator Cycle Sequencing Ready Reaction Kit v3.1 (Life Technologies, Darmstadt, Germany) on an ABI 3130 sequencer (Applied Biosystems, Foster City, CA). Sequences were analyzed by using 4Peaks Software v1.7.2 (The Netherlands Cancer Institute, Amsterdam, The Netherlands), Lasergene software (DNAStar, Madison, WI), and by manual review. Sequences were compared with mouse germ line *Ig* gene sequences with International ImMunoGeneTics database.[17] In addition, the PCR products of 1 case were cloned with the TOPO TA Cloning Kit (Life Technologies), which resulted in 32 sequences. To generate genealogic trees, sequence analysis focused on the *IGHV* segment, starting within FR1. To exclude possible Taq errors, only mutations shown more than once were considered for analysis (see supplemental Data).

Results

To assess the role of *MYD88*$^{p.L265P}$ in B-cell lymphomagenesis, we generated a conditional *Myd88*$^{p.L252P}$ allele (*Myd88*$^{c\text{-}p.L252P}$) that is expressed from the endogenous locus upon Cre-mediated recombination (Figure 1A). Murine *Myd88*$^{p.L252P}$ is at the orthologous position of human *Myd88*$^{p.L265P}$. To verify Cre-inducible *Myd88*$^{p.L252P}$ expression, we derived murine embryonic fibroblasts (MEFs) from wild-type

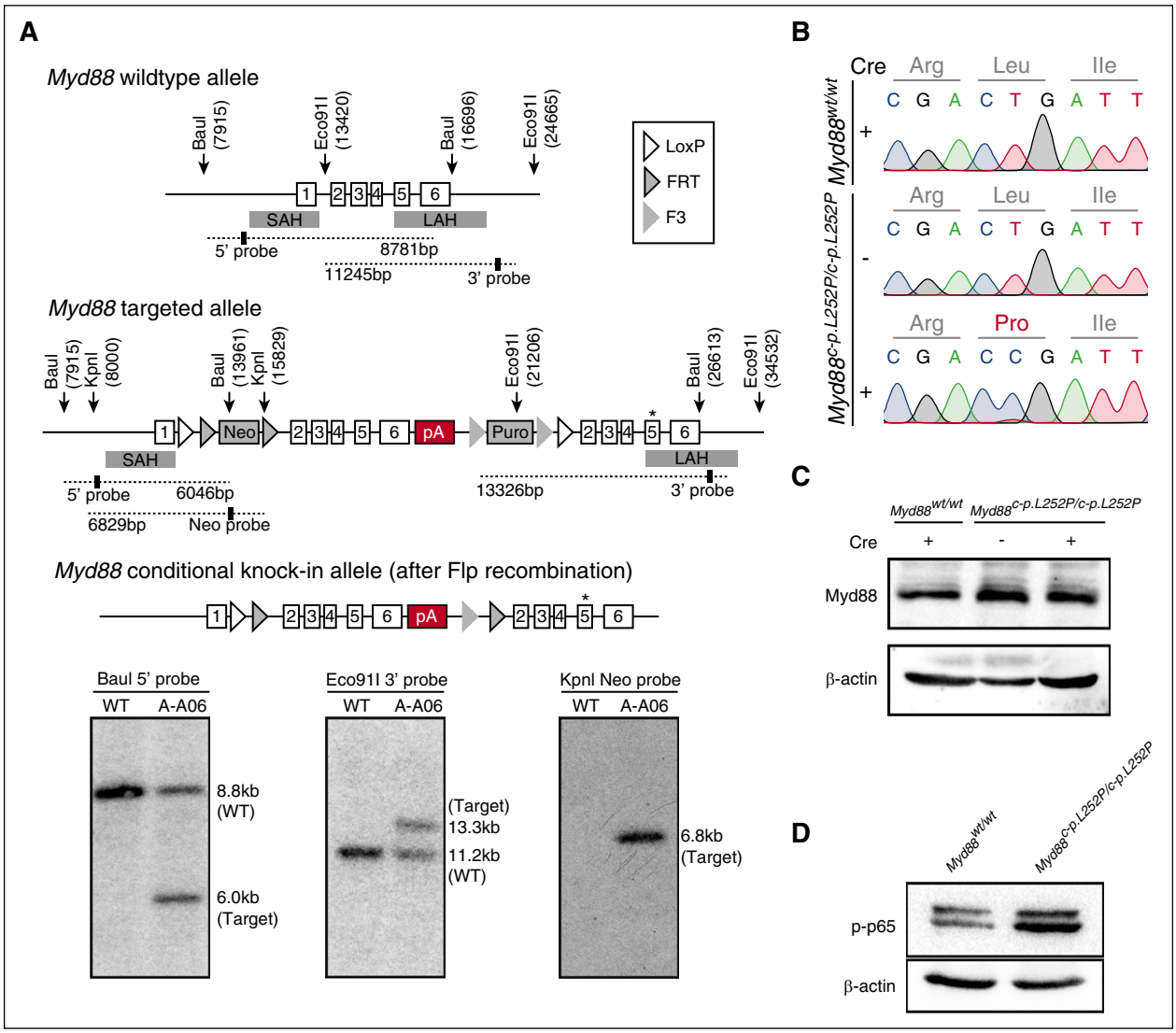

Figure 1. Construction of a conditional *Myd88*$^{p.L252P}$ allele. (A) Targeting of the *Myd88* locus in *C57BL/6N* Tac ES cells. The endogenous *Myd88* locus was targeted with the linearized vector described in the supplemental Data. The targeted allele before (middle panel) and after Flp-mediated recombination of FRT and F3 sites (bottom panel) is schematically depicted. The Southern blots of BaeI, Eco91I, and KpnI digested genomic DNA probed with a 5′, a 3′, and a Neo probe, respectively, are shown below the schematic illustration of the targeting strategy. Positions of restriction sites and probes are shown in the schematic drawing above. (B) *Myd88*$^{p.L252P}$ mRNA is expressed upon Cre-mediated recombination in MEFs. *Myd88*$^{wt/wt}$ and *Myd88*$^{c\text{-}p.L252P/c\text{-}p.L252P}$ MEFs were isolated. RNA was isolated from both cell lines before LentiCre application (Sanger sequencing chromatograms, top and middle panels) and the *Myd88* mRNA sequence was determined after reverse transcription. The wild-type sequence was recovered from both cell lines. After LentiCre application and puromycin selection, only the p.L252P sequence could be recovered from *Myd88*$^{c\text{-}p.L252P/c\text{-}p.L252P}$ MEFs (Sanger sequencing chromatogram, bottom panel). (C) The Myd88$^{p.L252P}$ isoform is expressed in *Myd88*$^{c\text{-}p.L252P/c\text{-}p.L252P}$ MEFs after LentiCre-mediated recombination. *Myd88*$^{wt/wt}$ and *Myd88*$^{c\text{-}p.L252P/c\text{-}p.L252P}$ MEFs were LentiCre exposed and puromycin selected, as in (B). Whole-cell lysates were separated on sodium dodecyl sulfate polyacrylamide gel electrophoresis (SDS-PAGE) and blotted onto polyvinylidene difluoride membranes before Myd88 and β-actin, which served as loading controls, and were visualized by immunoblotting. Both Myd88^{wt} and Myd88$^{p.L252P}$ proteins were expressed at equal levels. (D) Conditional LentiCre-mediated Myd88$^{p.L252P}$ expression leads to p65 Ser-536 phosphorylation. *Myd88*$^{wt/wt}$ and *Myd88*$^{c\text{-}p.L252P/c\text{-}p.L252P}$ MEFs were transduced with LentiCre and puromycin selected, as in (B). Upon selection, cells were lysed, proteins were separated on SDS-PAGE, and pSer-536 p65 was visualized by immunoblot. SAH, short arm of homology; LAH, long arm of homology; pA, polyadenylation signal sequence.

and *Myd88*$^{c\text{-}p.L252P/c\text{-}p.L252P}$ mice. By using Sanger sequencing, we detected expression of *Myd88*^{wt} messenger RNA (mRNA) in both *Myd88*$^{wt/wt}$ and *Myd88*$^{c\text{-}p.L252P/c\text{-}p.L252P}$ MEFs, indicating lack of background expression of *Myd88*$^{p.L252P}$ in the absence of Cre recombinase. In contrast, cytomegalovirus promoter-driven Cre expression mediated by lentiviral transduction of *Myd88*$^{c\text{-}p.L252P/c\text{-}p.L252P}$ MEFs induced recombination in the *Myd88* locus, leading to expression of *Myd88*$^{p.L252P}$-mutant mRNA (Figure 1B). Myd88 protein abundance was unaffected by stable Cre expression, indicating that the Myd88$^{p.L252P}$ isoform is expressed at endogenous levels (Figure 1C). This *Myd88*$^{p.L252P}$ expression translated into robust p65 Ser-536 phosphorylation, indicating activation of NF-κB signaling (Figure 1D).

To determine whether B-cell–specific *Myd88*$^{p.L252P}$ expression promotes lymphomagenesis, we compared *Cd19*$^{Cre/wt}$;*Myd88*$^{c\text{-}p.L252P/wt}$ (hereafter M-Cd19) and *Cd19*$^{Cre/wt}$ (hereafter Cd19) mice. The mice were longitudinally monitored by magnetic resonance imaging (MRI). Although no gross lymphoproliferative disease (LPD) was detectable in Cd19 mice, M-Cd19 mice developed splenomegaly and occasional lymphadenopathy starting at the age of ~60 weeks (Figure 2B). Similar MRI morphologic signs of LPD were observed when B-cell–specific *Myd88*$^{p.L252P}$ expression was induced by Cre

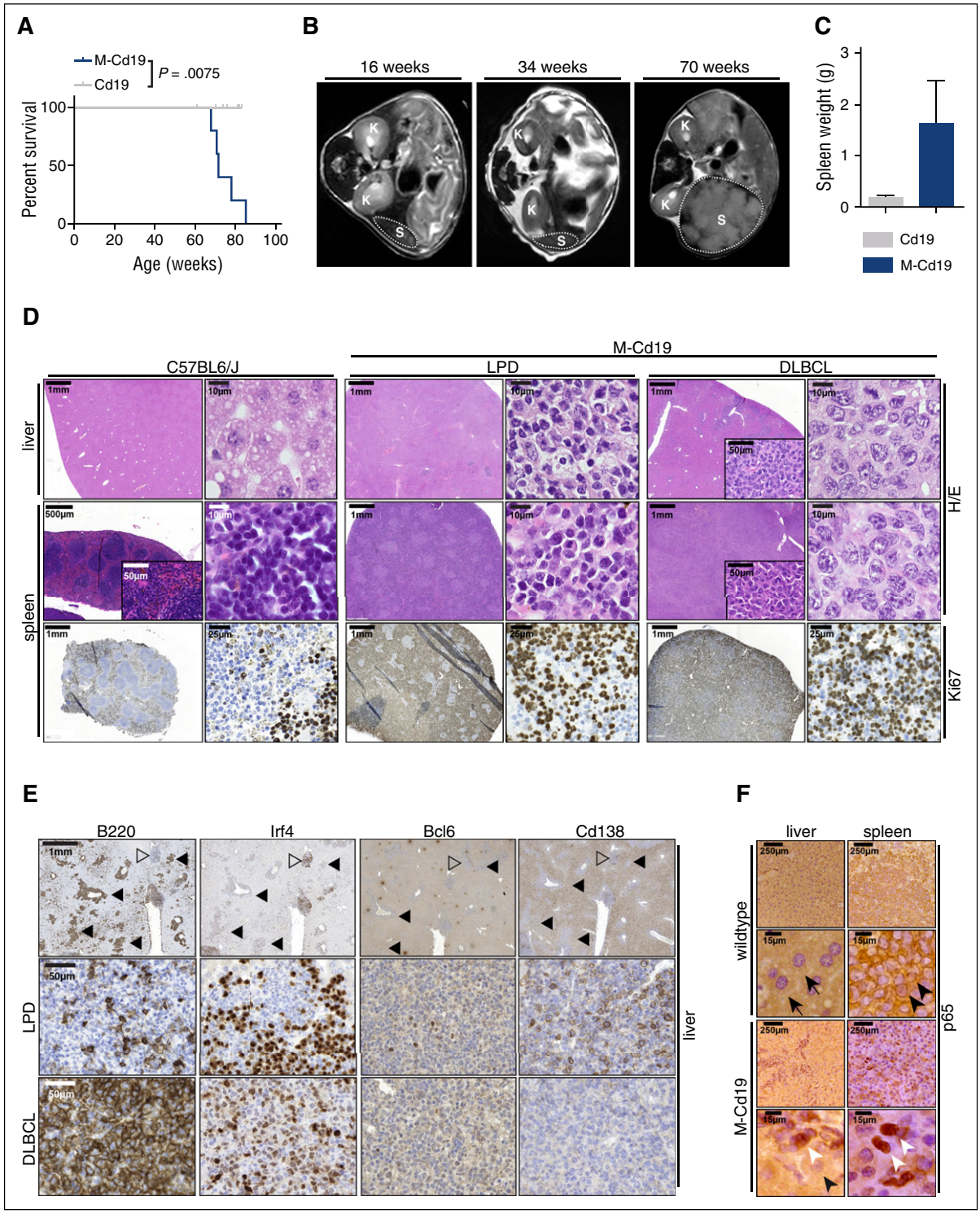

Figure 2. B-cell–specific *Myd88*$^{p.L252P}$ expression drives lymphoproliferation and lymphomagenesis in vivo. (A) B-cell–specific expression of *Myd88*$^{p.L252P}$ significantly reduces overall survival in vivo. Kaplan-Meier curves illustrate the overall survival of M-Cd19 mice. M-Cd19 mice display a significantly reduced survival compared with the respective controls (log-rank test). (B) Serial MRI scans in 16-, 34-, and 70-week-old M-Cd19 mice revealed the occurrence of splenomegaly in 70-week-old M-Cd19 mice. (C) M-Cd19 mice display splenomegaly at the time of death. Preterminal M-Cd19 and Cd19 mice were sacrificed and spleen weight was recorded. Bars represent the average (n = 3); error bars represent standard deviations. (D) M-Cd19 mice develop lymphoproliferative disease and occasional lymphoma. The top panels show H&E staining of spleens and livers isolated from *C57BL/6* and M-Cd19 mice at the time of death. Although the organ architecture appeared normal in *C57BL/6* wild-type mice, the architecture of spleens isolated from M-Cd19 mice was largely disrupted by infiltration of small mature lymphocytes (LPD columns) or large blastoid cells (DLBCL columns). The bottom panel shows the partial and complete disruption of the spleen by infiltrates with high proliferative indices. (E) Immunohistochemical characterization of the liver infiltrates of M-Cd19 mice. Areas of infiltrates morphologically resembling DLBCL (marked with solid triangles) showed a homogeneous staining pattern of B220 and Irf4 positivity, whereas they were negative for Bcl6 and Cd138 (bottom panel). Infiltrated areas of small, mature lymphocytes (marked with open triangles) displayed a more heterogeneous staining pattern of positive and negative cells for B220, Irf4, and Cd138, whereas staining was largely negative for Bcl6 (middle panel). (F) The lymphoma cells infiltrating spleens and livers of M-Cd19 mice displayed a largely nuclear localization of p65, indicating NF-κB activation. Black arrows indicate hepatocytes, black arrowheads indicate cytoplasmic p65 staining in splenic lymphocytes in *C57BL/6* wild-type mice, and white arrowheads indicate nuclear p65 staining in lymphoma cells in M-Cd19 mice.

expression that was driven off the *Aid* promoter (hereafter M-Aid), which is active in GCB cells, during both T cell–dependent and –independent immune responses (supplemental Figure 1A).[11,18] Furthermore, *Cd21* promoter-driven Cre, which is expressed when immature transitional B cells differentiate into mature long-lived peripheral B cells,[12] induced an LPD in $Cd21^{Cre/wt};Myd88^{c\text{-}p.L252P/wt}$ mice (hereafter M-Cd21) that was indistinguishable from that observed in M-Cd19 mice (supplemental Figure 1A).

The MRI morphologic occurrence of lymphoproliferative lesions translated into a significantly ($P = .0075$) reduced overall survival of M-Cd19 mice (median survival, 501 days) compared with Cd19 mice (median survival, not reached in 10 mice observed for 427 to 581 days [average, 539 days]) (Figure 2A). Similar data were obtained when Cre expression was driven off the *Aid* or *Cd21* promoter in M-Aid and M-Cd21 mice (median survival, 574 and 610 days, respectively) (supplemental Figure 1B). We noted that the majority of M-Cd19, M-Aid, and M-Cd21 mice included in this study displayed splenomegaly (4 of 4, M-Cd19; 2 of 3, M-Aid; and 2 of 3, M-Cd21), occasionally accompanied by macroscopic lymphadenopathy (1 of 4, M-Cd19; 2 of 3, M-Aid; and 1 of 3, M-Cd21). The strong oncogenic potential of the $Myd88^{p.L252P}$ mutation was also verified in an alternative mouse model of aggressive B-cell lymphoma in which $Myd88^{p.L252P}$ dramatically shortened tumor onset driven by oncogenic *Myc* (*Eμ:Myc* transgenic fetal liver cells transplanted into lethally irradiated recipient mice, stably transduced with either empty vector [n = 40; median onset not reached] or $Myd88^{p.L252P}$ [n = 12; median onset, 36 days]; log-rank Mantel-Cox $P < .0001$) (supplemental Figure 2).

To characterize the disease occurring in M-Cd19 mice, we initially performed histologic examinations. H&E staining of spleens and livers of M-Cd19, M-Aid, and M-Cd21 mice revealed infiltrates of lymphoid cells in these organs. In particular, the architecture of the spleens of these mice was largely disrupted by these infiltrates (4 of 4, M-Cd19; 3 of 3, M-Aid; 3 of 3, M-Cd21). Of note, we did not detect any infiltration of the bone marrow (n = 3 per genotype; supplemental Figure 3). Further analyses of the splenic and hepatic infiltrates revealed that these lesions constituted a largely monomorphic lymphoid cell population with indolent appearance, consistent with an LPD. Intriguingly, in a subset of mice (1 of 4, M-Cd19; 1 of 3, M-Aid; and 1 of 3, M-Cd21), diffuse large lymphoid infiltrates resembling DLBCL were detectable (Figure 2D; supplemental Figure 1D-E). Of note, the Ki-67 indices did not substantially differ between areas with LPD and DLBCL morphology (Figure 2D). To determine the clonality of these infiltrates, we next performed Southern blot analyses to detect clonal immunoglobulin (Ig) rearrangements. We were not able to detect clonal Ig rearrangements in genomic DNA isolated from areas with LPD-like appearance that were detected in M-Cd19, M-Aid, and M-Cd21 mice (supplemental Figure 4A). Strikingly, oligoclonal Ig rearrangement patterns were detected in DNA isolated from infiltrates that displayed DLBCL-like morphology in M-Cd19, M-Aid, and M-Cd21 mice (indicated by white triangles in supplemental Figure 4A). DNA isolated from spleens of an *Eμ:Tcl1*-driven CLL mouse model served as a positive control for the development of a clonal lymphoid neoplasm.[14] Altogether, our data strongly indicate that B-cell–specific $Myd88^{c\text{-}p.L252P}$ expression largely leads to an LPD, with only occasional development of mono-/oligoclonal lymphoma.

To further characterize the LPD and lymphomas, we next performed immunohistochemistry in liver infiltrates of M-Cd19 mice. As shown in Figure 2E, the areas with DLBCL-like morphology displayed a strikingly uniform staining pattern. These lesions were B220 and Irf4 positive and were Bcl6 and Cd138 negative, resembling the immunophenotype of a post-GCB lymphoid malignancy.[19] In contrast, the areas of LPD displayed a rather heterogeneous staining pattern for B220, Irf4, and Cd138 and were largely negative for Bcl6, further underscoring the nonclonal characteristics of these lesions. We noted that areas of LPD and DLBCL-like morphology in M-Aid and M-Cd21 mice displayed similar staining patterns (supplemental Figure 1F-G).

To further interrogate the nature of the DLBCL-like lesions, we next used immunohistochemistry to assess subcellular NF-κB localization, because constitutive NF-κB activation, indicated by nuclear enrichment, is a hallmark feature of ABC-DLBCL.[9] These experiments revealed a uniform nuclear staining of the NF-κB subunit p65 in the DLBCL-like lesions detected in spleens and livers of M-Cd19, M-Aid, and M-Cd21 mice (Figure 2F; supplemental Figure 1C). Given that ABC-DLBCL, which is characterized by constitutive NF-κB activation, carries the p.L265P mutation in 29% of the cases,[9] and given that the clonal lymphoproliferation we observed in M-Cd19 mice displayed morphologic features of DLBCL, we hypothesized that the B-cell–specific $Myd88^{c\text{-}p.L252P}$ expression drives ABC-DLBCL development in our model.

To cross-validate our observations, we analyzed *MYD88* mutation frequency in human DLBCLs (n = 24, GCB-DLBCL; n = 21, ABC-DLBCL). We performed targeted sequencing of FFPE-extracted DNA by multiplex PCR covering the *MYD88*, *ATM*, *BTK*, *CD79B*, *DDX3X*, *FBXW7*, *MAPK1*, *NOTCH1*, *PIK3CA*, *PIK3CD*, *PTEN*, *PTPN6*, *SF3B1*, *TP53*, and *XPO1* genes (Figure 3A). DLBCL subtypes were determined based on immunohistochemical stains for CD10, BCL6, and IRF4 following the Hans algorithm (Figure 3B).[19] The non-GCB of Hans algorithm was designated as "ABC" in our study. Confirming previously published data, we found a substantial overrepresentation of *MYD88* and *CD79B* mutations in ABC-DLBCLs compared with GCB-DLBCLs (Figure 3A,C; supplemental Table 1).[9,20,21] Furthermore, the anti-apoptotic oncogene *BCL2* is frequently deregulated in human DLBCL.[22,23] Whereas the chromosomal translocation t(14;18)(q32;q21), which juxtaposes *BCL2* and the *IGHV* enhancer, is commonly observed in GCB-DLBCL,[23] focal copy number gains are more commonly observed in ABC-DLBCL (~30% to 40%).[22-25] Indeed, mining of the whole-genome sequencing data on DLBCL from the German International Cancer Genome Consortium Molecular Mechanisms in Malignant Lymphoma by Sequencing Project (https://icgc.org/ and C.L., M.S., and R.S., manuscript in preparation) revealed that 6 DLBCLs carry the $MYD88^{p.L265P}$ mutation. Remarkably, all of these samples belonged to the ABC-DLBCL subtype and carried a copy number gain of 18q detected by both fluorescent in situ hybridization with a BCL2-specific probe and somatic copy number variant mapping.[26,27] A critical role for BCL2, particularly in activated B cells, is further corroborated by published transcriptome analyses. Specifically, *BCL2* mRNA was not expressed in GCB cells but was massively induced during activation of peripheral blood B cells.[28] Consistent with this, the majority of ABC-DLBCLs displayed *BCL2* mRNA levels more than fourfold higher than GCB cells.[28] Furthermore, exogenous expression of $MYD88^{p.L265P}$ in B cells was recently shown to induce the accumulation of self-reactive B cells in vivo only when apoptosis was opposed by *Bcl2* overexpression.[29] Additional circumstantial evidence suggesting that ABC-DLBCL in particular might depend on functional *BCL2* activity could be derived from recently published, large-scale in vitro drug sensitivity profiling experiments. Specifically, re-assessment of a data set published by Stegmeier and colleagues revealed that *MYD88*-mutant DLBCLs in particular display an actionable BCL2 addiction, which could be exploited by the targeted high-affinity BCL2 inhibitor ABT-263 (supplemental Figure 5A-B).[30] The BTK inhibitor ibrutinib was recently shown to synergistically interact with the BCL2 family inhibitor navitoclax (ABT-263) in killing ABC-DLBCL cells.[31] We

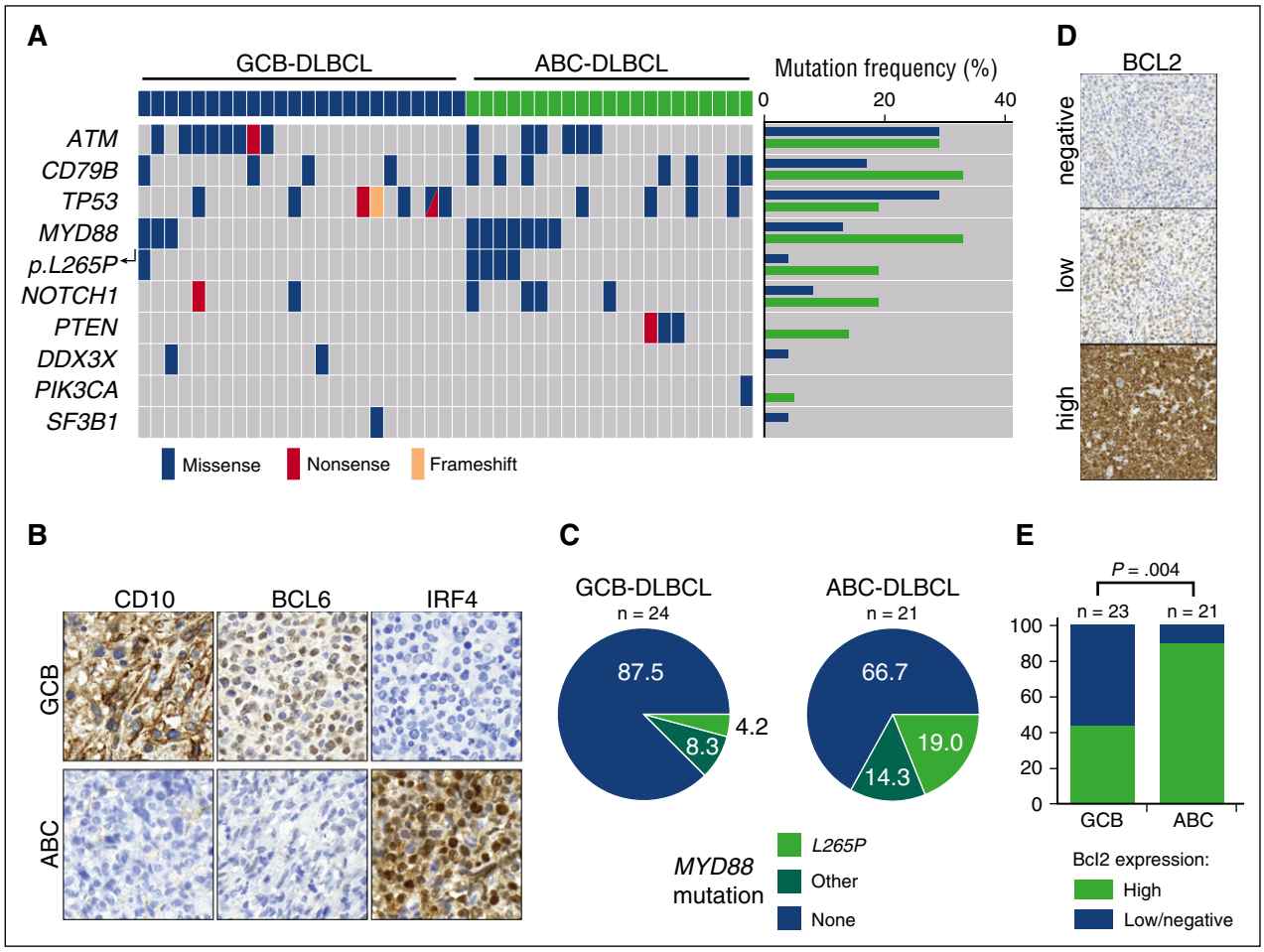

Figure 3. *MYD88* mutations and high expression of BCL2 are enriched in ABC-DLBCL. (A) *MYD88* mutations are substantially enriched in human ABC-DLBCL. Human DLBCLs were stratified as ABC- or GCB-DLBCL following the Hans algorithm, as depicted in (B). After immunohistochemistry-based stratification, DNA was isolated from tissue sections and subjected to targeted deep sequencing by a multiplex PCR, which covered the *ATM*, *BTK*, *CD79B*, *DDX3X*, *FBXW7*, *MAPK1*, *MYD88*, *NOTCH1*, *PIK3CA*, *PIK3CD*, *PTEN*, *PTPN6*, *SF3B1*, *TP53*, and *XPO1* genes. *MYD88* mutations per se, and particularly the *MYD88*$^{p.L265P}$ mutation were substantially enriched in ABC-DLBCL. Similarly, *CD79B* and *PTEN* mutations were enriched in ABC-DLBCL. (C) Distribution of *MYD88* mutations detected in human DLBCL samples is shown in pie charts. The samples were classified into high and low or negative expression of BCL2, as shown in (D). (E) High protein expression levels of BCL2 are significantly enriched in ABC-DLBCL (Fisher's exact test).

validated these observations in our cohort of DLBCL samples by using immunohistochemistry to assess BCL2 expression. As shown in Figure 3D-E, high-level BCL2 expression was significantly enriched in ABC-DLBCL patients compared with patients who had GCB-DLBCL. Altogether, these genomic, transcriptomic, immunohistochemical, and functional data strongly suggest that enhanced *BCL2* activity plays a central pathomechanistic role in the development of ABC-DLBCL. On the basis of these considerations, we next asked whether lymphoma development in M-Cd19 mice could be accelerated by increased *BCL2* gene dosage in vivo. To mimic *BCL2* amplification in vivo, we generated a novel conditional allele in which *BCL2.IRES.GFP* was targeted into the *Rosa26* locus. *BCL2* expression was prevented by the insertion of a *LoxP.STOP.LoxP* cassette upstream of the translation-initiating codon (supplemental Figure 5C). By using this allele, we generated *Cd19*$^{Cre/wt}$;*Rosa26*$^{LSL.BCL2.IRES.GFP/wt}$;*Myd88*$^{c\text{-}p.L252P/wt}$ mice (hereafter M-B-Cd19), in which *Cd19*-driven Cre mediates the excision of the *LoxP.STOP.LoxP* cassette from the *Rosa26* locus, leading to CAGS-promoter-driven *BCL2* overexpression in addition to *Myd88*$^{p.L252P}$ expression. MRI scans revealed that M-B-Cd19 mice developed splenomegaly substantially earlier than M-Cd19, M-Aid, or M-Cd21 mice (Figures 2B and 4B; supplemental Figure 1A). Furthermore, M-B-Cd19 mice displayed a significantly reduced overall survival (median survival, 179 days) compared with M-Cd19, M-Aid, and M-Cd21 mice (long-rank $P = .0008$, $P = .0001$, and $P < .0001$, respectively) (Figure 4A). Of note, all of the M-B-Cd19 mice displayed excessive lymphadenopathy and/or splenomegaly at the time of death (splenomegaly in 7 of 8 mice; lymphadenopathy in 6 of 8 mice).

To further characterize the nature of the lymphadenopathy that we observed in M-B-Cd19 mice by MRI, we next performed histologic examination of infiltrated organs (livers, lymph nodes, and spleens). Morphologic assessment of the splenic, hepatic, and lymph node lesions detected in M-B-Cd19 mice revealed that these infiltrates consisted almost entirely of diffuse large lymphoid cells with blastoid to plasmablastoid appearance (Figure 4C). Intriguingly, plasmablasts have been implicated as the cell of origin of ABC-DLBCL.[24] In marked contrast to the phenotype observed in M-Cd19 mice, in which the bulk of the lesions consisted of LPD-like infiltrates (Figure 2D), areas of LPD were only rarely detectable in M-B-Cd19 mice. Furthermore, the Ki-67 index of the lymphoid lesions in M-B-Cd19 mice was significantly higher compared with lesions that emerged in M-Cd19 mice (median, 71.57% ± 3.65% in M-B-Cd19 mice vs 28.27% ± 2.40% in M-Cd19 mice) (Figure 4F). The Ki-67 indices observed in M-B-Cd19 mice

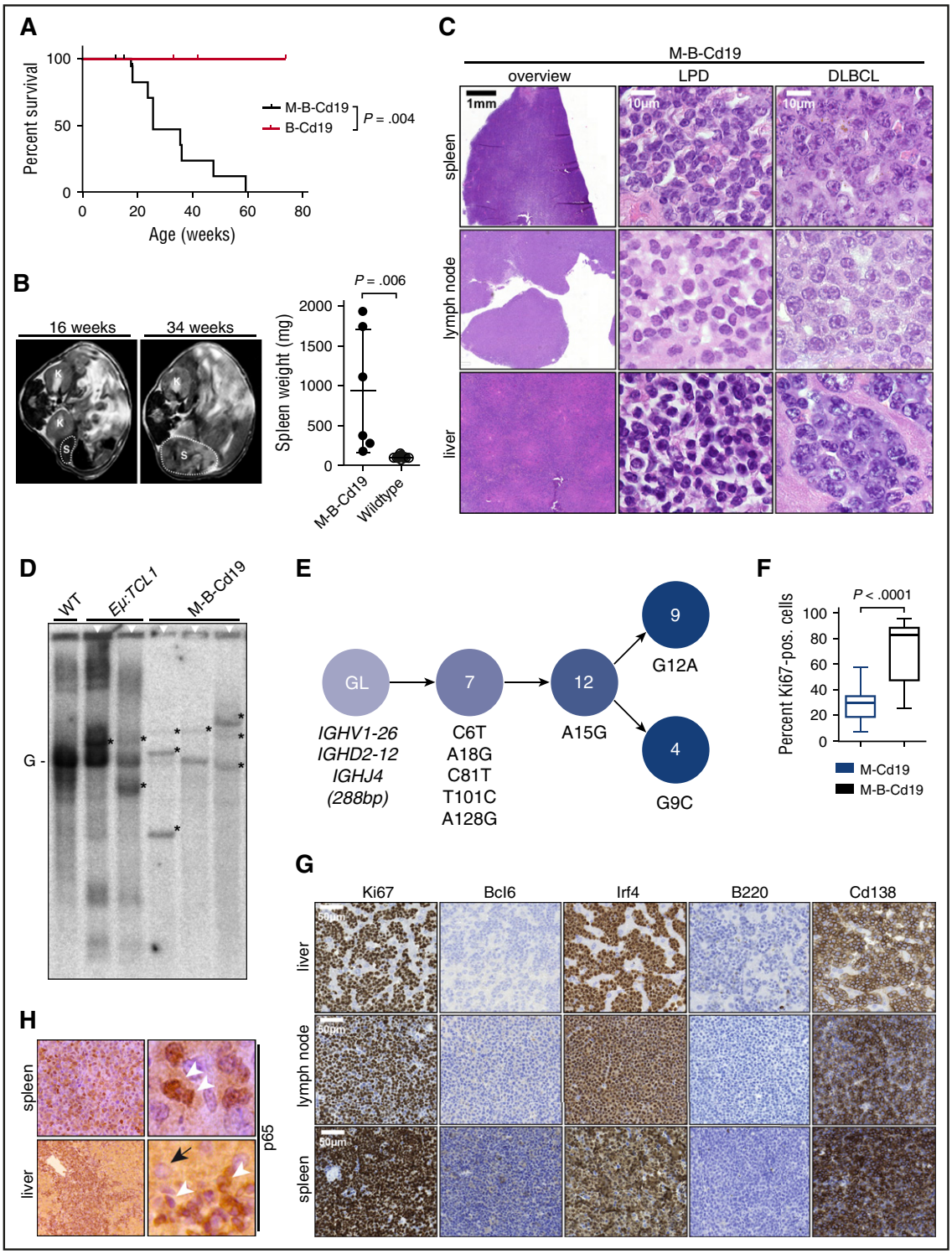

Figure 4. Combination of B-cell–specific *BCL2* overexpression and *Myd88*$^{p.L252P}$ expression drives ABC-DLBCL development in vivo. (A) Kaplan-Meier curve illustrates overall survival of M-B-Cd19 mice. M-B-Cd19 mice display a significantly reduced survival compared with the respective controls (log-rank test). (B) M-B-Cd19 mice develop splenomegaly at 25 to 35 weeks. MRI scans and quantification of spleen weights at autopsy are shown (two-tailed Student *t* test). (C) The architecture of spleens and lymph nodes isolated from M-B-Cd19 mice was completely disrupted by a homogeneous infiltrating population of large lymphoblastoid cells (DLBCL column). Small areas of more heterogeneous lymphoid cell populations consisting of small lymphoid cells were occasionally detectable (LPD column). The livers of M-B-Cd19 mice were diffusely infiltrated by large blastoid cells with DLBCL-like morphology. (D) Variable-diversity-joining–recombination analysis by Southern blot analysis revealed the presence of clonal populations in tumors of M-B-Cd19 mice. Tumors from leukemic *Eμ:TCL1* mice were used as oligoclonal controls. The germ line configuration is also present in the WT controls and is depicted as "G." Asterisks indicate clonal rearrangements. Samples of mice with lymphoma detected by histologic analyses are marked with white triangles (top). (E) Genealogic trees of murine DLBCL isolated from M-B-Cd19 mice. *Igh* rearrangements were cloned and individual clones were sequenced. Analysis focused on the *Ighv* segments starting with FR1. Genealogic tree was derived from 32 sequences. The tree-like structures demonstrate ongoing somatic hypermutation. Numbers in circles show number of sequence reads; numbering of mutations is in regard to the germ line sequence of *Ighv1-26*. (F) The Ki-67 index of DLBCL lesions from M-B-Cd19 mice was significantly higher than that in M-Cd19 mice ($P = 2.27 \times 10^{-12}$, two-tailed Student *t* test; n = 3 mice per genotype; 20 fields of view per lesion). (G) Lymphoma infiltrates of M-B-Cd19 mice were immunohistochemically analyzed and stained positive for Irf4 and Cd138 and negative for B220 and Bcl6. The Ki-67 stainings are quantified in (F).

matched those typically detected in aggressive human lymphoma.[32] Leukemic effusion was detectable only in M-B-Cd19 mice (supplemental Figure 6).

Consistent with the monomorphic appearance of the blastoid lesions detected in M-B-Cd19 mice, clonality analyses using Southern blot to detect Ig rearrangements revealed that these infiltrates were of clonal or oligoclonal origin (3 of 3 lesions isolated from independent mice) (Figure 4D). Expression of the mutant *Myd88* allele in the lymphomas was verified by reverse transcriptase PCR sequencing analysis (supplemental Figure 7). To ask whether the oligoclonal lymphomas underwent somatic hypermutation, as would be expected in the case of ABC-DLBCL, we analyzed a clonal lesion for *Igh* rearrangements by direct sequencing. As shown in Figure 4E, we could detect a clonal *Ighv1-26*, *Ighd2-12*, *Ighj4* rearrangement. The sequence shows an in-frame rearrangement with mutations but no stop-codons. Thus, this rearrangement is potentially functional. Next, we cloned the amplified *Ighv* gene rearrangements from this sample and sequenced 32 subclones to investigate intraclonal diversity. All analyzed sequences shared 5 mutations compared with the most homologous germ line sequence (*Ighv1-26*). Further mutations could be detected in several subclones (Figure 4E), demonstrating intraclonal diversity for this analyzed case.

Next, we used immunohistochemistry to further characterize the lymphomas isolated from M-B-Cd19 mice. As shown in Figure 4G and supplemental Figure 8, the lesions stained uniformly positive for Irf4 and were entirely negative for Bcl6, consistent with the somatic hypermutation detected in Figure 4E and further corroborating the post-germinal center (GC) nature of the infiltrates.[24] Furthermore, the lymphomas lost B220 expression and stained strongly positive for Cd138, indicating ABC origin of these lesions.[33-36] This is in line with analyses of human DLBCL, which indicate that GC-experienced Cd138-positive non-GC-DLBCLs are typically of plasmablastoid differentiation.[37-39] In agreement with constitutive NF-κB activation, which is typically observed in human ABC-DLBCL, we found almost exclusive nuclear p65 staining in the lymphomas detected in M-B-Cd19 mice (Figure 4H).

Although *MYD88* mutations have not been detected in human multiple myeloma,[8,40-42] the strong Cd138 positivity of the lymphomas growing in M-B-Cd19 mice suggested the possibility that these lesions might be of plasmacellular origin.[8,40-42] However, despite considerable effort, we were unable to detect a plasma cell expansion in the bone marrow of M-Cd19, M-Aid, M-Cd21, and M-B-Cd19 mice. More importantly, we did not find lymphoma infiltration of the bone marrow in M-Cd19, M-Aid, and M-Cd21 mice, and only 1 of 4 M-B-Cd19 mice showed an isolated lymphoma infiltrate that did not display signs of plasmacellular differentiation (supplemental Figures 3 and 9). In line with a lack of a consistent bone marrow infiltration, which is an obligatory feature of Waldenström macroglobulinemia and is frequently observed in multiple myeloma, we did not detect mono- or oligoclonal gammopathy in either M-Cd19 or M-B-Cd19 mice (supplemental Figure 10). However, we did detect an increased abundance of the Ig fraction in M-Cd19 mice compared with wild-type controls by using serum electrophoresis (upper and middle panels of supplemental Figure 10). This gammopathy was even more prominent in M-B-Cd19 mice (lower panel of supplemental Figure 10). The overall polyclonality strongly suggests a non-neoplastic origin of the gammopathy observed in M-Cd19 and M-B-Cd19 mice. Thus in summary, the morphologic appearance, as well as the immunophenotype of the lesions observed in M-B-Cd19 mice strongly suggests that these lymphomas represent ABC-DLBCL.

Discussion

Here, we generated a novel conditional *Myd88*$^{p.L252P}$ allele, which is at the orthologous position of the human *Myd88*$^{p.L265P}$ mutation and is expressed from the endogenous locus upon Cre-mediated recombination. We chose to design an allele that allows expression outside the natural genomic context to most faithfully mimic the situation in human malignancies. B cell–specific expression of this mutant leads to an LPD and occasional (~30%) transformation into an aggressive lymphoma that morphologically and immunophenotypically resembles human ABC-DLBCL. Interestingly, development of LPD and lymphoma occurred at a similar rate, regardless of the Cre allele. We specifically used a pan B-cell Cre allele (*Cd19*^{Cre}), a Cre allele that is active in GCB cells (*Aid*^{Cre}), and a Cre allele that is expressed when immature transitional B cells differentiate into mature peripheral B cells (*Cd21*^{Cre}). These data might indicate that *Myd88*$^{p.L252P}$ expression leads to a block in B-cell differentiation after the GC reaction. Consistent with this postgerminal nature of *Myd88*$^{p.L252P}$-expressing cells, we find that the resulting lymphomas are consistently Bcl6 negative and express Irf4 (Figure 2E; supplemental Figure 1F-G). These observations are in line with data from human lymphoma patients, which suggests that oncogenic *MYD88* mutations are enriched in post-GC malignancies, such as ABC-DLBCL, Waldenström macroglobulinemia, and the *IGHV*-mutant GC-experienced subset of CLL patients.[7-9,24,43-45] Furthermore, crossing in an additional allele that allows conditional *BCL2* expression from the *Rosa26* locus leads to 100%-penetrant development of ABC-DLBCL.

Both *MYD88*[46-48] and *BCL2*[24,49-51] have been shown to be critical for transition through the GC. Thus, it is conceivable that mice displaying B-cell–specific *Myd88*$^{p.L252P}$ expression (M-Cd19) or *Myd88*$^{p.L252P}$ expression in combination with *BCL2* overexpression (M-B-Cd19) might accumulate post-GCB cells. Consistent with this, we find a polyclonal gammopathy in both M-Cd19 and M-B-Cd19 mice (supplemental Figure 10).

MYD88 is frequently mutated in ~29% of ABC-DLBCL cases.[9] However, *MYD88* mutations are even more common in Waldenström macroglobulinemia, in which these alterations are detected in ~90% of the cases.[8,52] Thus, it is somewhat surprising that our *Myd88*$^{p.L252P}$-expressing mice develop clonal ABC-DLBCL rather than Waldenström macroglobulinemia. One possible explanation might be the different genomic landscapes of these distinct B-cell neoplasias. For instance, mutations in the carboxyl terminal domain of the chemokine receptor CXCR4 have been detected in a substantial portion of patients with Waldenström macroglobulinemia (~30% of the patients), whereas they are absent in ABC-DLBCL.[2,9,53] Furthermore, somatic mutations affecting *CD79A* and *CD79B* are present in ~20% of human ABC-DLBCLs, whereas these alterations are rare or absent in other lymphoma entities.[20,24] Thus, it will be interesting to combine our novel *Myd88*$^{p.L252P}$ allele with additional B-cell–specific genetic alterations to determine whether further manipulation might enable a plasmacytoid differentiation.

Our novel models represent a preclinical platform that could be exploited for the in vivo development and validation of novel therapeutic approaches to treat ABC-DLBCL, which remains a difficult-to-treat clinical entity.[54,55] For instance, it will be interesting to see whether combined targeting of the apoptotic machinery and the myddosome, through BCL2 inhibition and IRAK4 repression, will result in synergistic toxicity in *Myd88*-driven ABC-DLBCL.[55] Our models might also serve to delineate the potential role of NF-κB and MAPKK6 signaling as actionable pathways downstream of the myddosome

complex in ABC-DLBCL.[56] For this purpose, it will be interesting to assess the cytotoxic potential of TAK1, IkB kinase, and MAPKK6 inhibitors in our *Myd88*-driven models of ABC-DLBCL. Altogether, we demonstrated the oncogenic role of a novel $Myd88^{p.L252P}$ allele in B-cell neoplastic disease in vivo. The resulting autochthonous mouse models of ABC-DLBCL represent useful preclinical tools for the development, validation, and refinement of novel treatment strategies for ABC-DLBCL in the clinical arena.

Acknowledgments

The authors are indebted to their patients, who provided primary material. The authors thank Alexandra Florin, Marion Müller, and Ursula Rommerscheidt-Fuss (Institute of Pathology, University Hospital Cologne) for their outstanding technical support.

This work was supported by the Volkswagenstiftung (Lichtenberg Program [H.C.R.]), the Deutsche Forschungsgemeinschaft (KFO-286 [H.C.R., H.K., F.T.W., and L.P.F.], KA 2853/4-1 [H.K.], and SFB-685 [A.N.R.W., O.-O.W.]), the Deutsche Jose Carreras Leukämie Stiftung (R12/26 [H.C.R. and L.P.F.]), the Marga und Walter Boll Stiftung (210-05-13 [L.P.F.]), the Helmholtz-Gemeinschaft (Preclinical Comprehensive Cancer Center [H.C.R. and C.A.S.]), the Else Kröner-Fresenius Stiftung (EKFS-2014-A06 [H.C.R.]), the Marlene Porsche Foundation for Cancer Prevention (S.B.), the Else-Übelmesser Stiftung (Juniorprofessoren-Programn [A.N.R.W]), the Deutsche Krebshilfe (111724 [H.C.R.]), and the German Ministry of Science and Education in the framework of the International Cancer Genome Consortium Molecular Mechanisms in Malignant Lymphoma by Sequencing Project (01KU1002A-J [C.L., P.M., L.T., and R.S.]).

Authorship

Contribution: H.C.R. conceived and supervised the experiments and wrote the manuscript; L.P.F., H.K., M.A.-M., J.M.S., R.B., and F.T.W. provided mouse strains and materials; T.P. and Y.A.-B. performed magnetic resonance imaging scans and volumetric analyses; G.K., S.C.S., K.V., M.P., S.B., P.L., P.M., M. Ortmann, and R.B. performed immunohistochemistry and pathologic analyses; and L.M.S., A.N.R.W., O.-O.W., A.H.S., A.R.K., G.K., P.L., D.K., M. Odenthal, C.F., C.A.S., M.M.-R., M.R., M.A.-M., M.S., C.L., L.T., and R.S. performed experiments.

Conflict-of-interest disclosure: The authors declare no competing financial interests.

A full list of members and affiliations of the German International Cancer Genome Consortium Molecular Mechanisms in Malignant Lymphoma by Sequencing Project Consortium appears in the supplemental Data.

Correspondence: H. Christian Reinhardt, Department I of Internal Medicine, University Hospital of Cologne, Weyertal 115B, 50931 Cologne, Germany; e-mail: christian.reinhardt@uk-koeln.de.

References

1. Akira S, Takeda K. Toll-like receptor signalling. *Nat Rev Immunol.* 2004;4(7):499-511.
2. Compagno M, Lim WK, Grunn A, et al. Mutations of multiple genes cause deregulation of NF-kappaB in diffuse large B-cell lymphoma. *Nature.* 2009;459(7247):717-721.
3. Loiarro M, Volpe E, Ruggiero V, et al. Mutational analysis identifies residues crucial for homodimerization of myeloid differentiation factor 88 (MyD88) and for its function in immune cells. *J Biol Chem.* 2013;288(42):30210-30222.
4. Lin SC, Lo YC, Wu H. Helical assembly in the MyD88-IRAK4-IRAK2 complex in TLR/IL-1R signalling. *Nature.* 2010;465(7300):885-890.
5. Ye H, Arron JR, Lamothe B, et al. Distinct molecular mechanism for initiating TRAF6 signalling. *Nature.* 2002;418(6896):443-447.
6. Xia ZP, Sun L, Chen X, et al. Direct activation of protein kinases by unanchored polyubiquitin chains. *Nature.* 2009;461(7260):114-119.
7. Puente XS, Pinyol M, Quesada V, et al. Whole-genome sequencing identifies recurrent mutations in chronic lymphocytic leukaemia. *Nature.* 2011; 475(7354):101-105.
8. Treon SP, Xu L, Yang G, et al. MYD88 L265P somatic mutation in Waldenström's macroglobulinemia. *N Engl J Med.* 2012;367(9): 826-833.
9. Ngo VN, Young RM, Schmitz R, et al. Oncogenically active MYD88 mutations in human lymphoma. *Nature.* 2011;470(7332):115-119.
10. Rickert RC, Roes J, Rajewsky K. B lymphocyte-specific, Cre-mediated mutagenesis in mice. *Nucleic Acids Res.* 1997;25(6):1317-1318.
11. Robbiani DF, Bothmer A, Callen E, et al. AID is required for the chromosomal breaks in c-myc that lead to c-myc/IgH translocations. *Cell.* 2008; 135(6):1028-1038.
12. Kraus M, Alimzhanov MB, Rajewsky N, Rajewsky K. Survival of resting mature B lymphocytes depends on BCR signaling via the Igalpha/beta heterodimer. *Cell.* 2004;117(6):787-800.
13. Riabinska A, Daheim M, Herter-Sprie GS, et al. Therapeutic targeting of a robust non-oncogene addiction to PRKDC in ATM-defective tumors. *Sci Transl Med.* 2013;5(189):189ra78.
14. Bichi R, Shinton SA, Martin ES, et al. Human chronic lymphocytic leukemia modeled in mouse by targeted TCL1 expression. *Proc Natl Acad Sci USA.* 2002;99(10):6955-6960.
15. Schmitt CA, Fridman JS, Yang M, Baranov E, Hoffman RM, Lowe SW. Dissecting p53 tumor suppressor functions in vivo. *Cancer Cell.* 2002; 1(3):289-298.
16. Montesinos-Rongen M, Sánchez-Ruiz M, Brunn A, et al. Mechanisms of intracerebral lymphoma growth delineated in a syngeneic mouse model of central nervous system lymphoma. *J Neuropathol Exp Neurol.* 2013;72(4):325-336.
17. Lefranc MP, Giudicelli V, Ginestoux C, et al. IMGT, the international ImMunoGeneTics information system. *Nucleic Acids Res.* 2009; 37(Database issue):D1006-D1012.
18. Crouch EE, Li Z, Takizawa M, et al. Regulation of AID expression in the immune response. *J Exp Med.* 2007;204(5):1145-1156.
19. Hans CP, Weisenburger DD, Greiner TC, et al. Confirmation of the molecular classification of diffuse large B-cell lymphoma by immunohistochemistry using a tissue microarray. *Blood.* 2004;103(1):275-282.
20. Davis RE, Ngo VN, Lenz G, et al. Chronic active B-cell-receptor signalling in diffuse large B-cell lymphoma. *Nature.* 2010;463(7277):88-92.
21. Kim Y, Ju H, Kim DH, et al. CD79B and MYD88 mutations in diffuse large B-cell lymphoma. *Hum Pathol.* 2014;45(3):556-564.
22. Dierlamm J, Murga Penas EM, Bentink S, et al; Deutsche Krebshilfe Network Project "Molecular Mechanisms in Malignant Lymphomas". Gain of chromosome region 18q21 including the MALT1 gene is associated with the activated B-cell-like gene expression subtype and increased BCL2 gene dosage and protein expression in diffuse large B-cell lymphoma. *Haematologica.* 2008;93(5):688-696.
23. Testoni M, Zucca E, Young KH, Bertoni F. Genetic lesions in diffuse large B-cell lymphomas. *Ann Oncol.* 2015;26(6):1069-1080.
24. Rui L, Schmitz R, Ceribelli M, Staudt LM. Malignant pirates of the immune system. *Nat Immunol.* 2011;12(10):933-940.
25. Lenz G, Wright GW, Emre NC, et al. Molecular subtypes of diffuse large B-cell lymphoma arise by distinct genetic pathways. *Proc Natl Acad Sci USA.* 2008;105(36):13520-13525.
26. Richter J, Schlesner M, Hoffmann S, et al; ICGC MMML-Seq Project. Recurrent mutation of the ID3 gene in Burkitt lymphoma identified by integrated genome, exome and transcriptome sequencing. *Nat Genet.* 2012;44(12):1316-1320.
27. Kretzmer H, Bernhart SH, Wang W, et al; ICGC MMML-Seq project; BLUEPRINT project. DNA methylome analysis in Burkitt and follicular lymphomas identifies differentially methylated regions linked to somatic mutation and transcriptional control. *Nat Genet.* 2015;47(11): 1316-1325.
28. Alizadeh AA, Eisen MB, Davis RE, et al. Distinct types of diffuse large B-cell lymphoma identified by gene expression profiling. *Nature.* 2000; 403(6769):503-511.
29. Wang JQ, Jeelall YS, Beutler B, Horikawa K, Goodnow CC. Consequences of the recurrent MYD88(L265P) somatic mutation for B cell tolerance. *J Exp Med.* 2014;211(3):413-426.
30. Rahal R, Frick M, Romero R, et al. Pharmacological and genomic profiling identifies NF-κB-targeted treatment strategies for mantle cell lymphoma. *Nat Med.* 2014;20(1):87-92.

31. Mathews Griner LA, Guha R, Shinn P, et al. High-throughput combinatorial screening identifies drugs that cooperate with ibrutinib to kill activated B-cell-like diffuse large B-cell lymphoma cells. *Proc Natl Acad Sci USA.* 2014; 111(6):2349-2354.
32. Salles G, de Jong D, Xie W, et al. Prognostic significance of immunohistochemical biomarkers in diffuse large B-cell lymphoma: a study from the Lunenburg Lymphoma Biomarker Consortium. *Blood.* 2011;117(26):7070-7078.
33. Tan LH. A practical approach to the understanding and diagnosis of lymphoma: an assessment of the WHO classification based on immunoarchitecture and immuno-ontogenic principles. *Pathology.* 2009;41(4):305-326.
34. Bai M, Skyrlas A, Agnantis NJ, et al. B-cell differentiation, apoptosis and proliferation in diffuse large B-cell lymphomas. *Anticancer Res.* 2005;25(1A):347-362.
35. Fournier EM, Velez MG, Leahy K, et al. Dual-reactive B cells are autoreactive and highly enriched in the plasmablast and memory B cell subsets of autoimmune mice. *J Exp Med.* 2012; 209(10):1797-1812.
36. Coro ES, Chang WL, Baumgarth N. Type I IFN receptor signals directly stimulate local B cells early following influenza virus infection. *J Immunol.* 2006;176(7):4343-4351.
37. Chang CC, McClintock S, Cleveland RP, et al. Immunohistochemical expression patterns of germinal center and activation B-cell markers correlate with prognosis in diffuse large B-cell lymphoma. *Am J Surg Pathol.* 2004;28(4): 464-470.
38. Colomo L, López-Guillermo A, Perales M, et al. Clinical impact of the differentiation profile assessed by immunophenotyping in patients with diffuse large B-cell lymphoma. *Blood.* 2003; 101(1):78-84.
39. Said JW. Aggressive B-cell lymphomas: how many categories do we need? *Mod Pathol.* 2013; 26(Suppl 1):S42-S56.
40. Mori N, Ohwashi M, Yoshinaga K, et al. L265P mutation of the MYD88 gene is frequent in Waldenström's macroglobulinemia and its absence in myeloma. *PLoS One.* 2013;8(11): e80088.
41. Xu L, Hunter ZR, Yang G, et al. MYD88 L265P in Waldenström macroglobulinemia, immunoglobulin M monoclonal gammopathy, and other B-cell lymphoproliferative disorders using conventional and quantitative allele-specific polymerase chain reaction. *Blood.* 2013;121(11): 2051-2058.
42. Jiménez C, Sebastián E, Chillón MC, et al. MYD88 L265P is a marker highly characteristic of, but not restricted to, Waldenström's macroglobulinemia. *Leukemia.* 2013;27(8): 1722-1728.
43. Landau DA, Carter SL, Stojanov P, et al. Evolution and impact of subclonal mutations in chronic lymphocytic leukemia. *Cell.* 2013;152(4): 714-726.
44. Landau DA, Tausch E, Taylor-Weiner AN, et al. Mutations driving CLL and their evolution in progression and relapse. *Nature.* 2015; 526(7574):525-530.
45. Quesada V, Conde L, Villamor N, et al. Exome sequencing identifies recurrent mutations of the splicing factor SF3B1 gene in chronic lymphocytic leukemia. *Nat Genet.* 2011;44(1):47-52.
46. Hua Z, Gross AJ, Lamagna C, et al. Requirement for MyD88 signaling in B cells and dendritic cells for germinal center anti-nuclear antibody production in Lyn-deficient mice. *J Immunol.* 2014;192(3):875-885.
47. Hou B, Saudan P, Ott G, et al. Selective utilization of Toll-like receptor and MyD88 signaling in B cells for enhancement of the antiviral germinal center response. *Immunity.* 2011;34(3):375-384.
48. Meyer-Bahlburg A, Khim S, Rawlings DJ. B cell intrinsic TLR signals amplify but are not required for humoral immunity. *J Exp Med.* 2007;204(13): 3095-3101.
49. Saito M, Novak U, Piovan E, et al. BCL6 suppression of BCL2 via Miz1 and its disruption in diffuse large B cell lymphoma. *Proc Natl Acad Sci USA.* 2009;106(27):11294-11299.
50. Ci W, Polo JM, Cerchietti L, et al. The BCL6 transcriptional program features repression of multiple oncogenes in primary B cells and is deregulated in DLBCL. *Blood.* 2009;113(22): 5536-5548.
51. Smith KG, Light A, O'Reilly LA, Ang SM, Strasser A, Tarlinton D. bcl-2 transgene expression inhibits apoptosis in the germinal center and reveals differences in the selection of memory B cells and bone marrow antibody-forming cells. *J Exp Med.* 2000;191(3):475-484.
52. Kapoor P, Paludo J, Vallumsetla N, Greipp PR. Waldenström macroglobulinemia: What a hematologist needs to know. *Blood Rev.* 2015; 29(5):301-319.
53. Hunter ZR, Xu L, Yang G, et al. The genomic landscape of Waldenstrom macroglobulinemia is characterized by highly recurring MYD88 and WHIM-like CXCR4 mutations, and small somatic deletions associated with B-cell lymphomagenesis. *Blood.* 2014;123(11):1637-1646.
54. Tilly H, Gomes da Silva M, Vitolo U, et al; ESMO Guidelines Committee. Diffuse large B-cell lymphoma (DLBCL): ESMO Clinical Practice Guidelines for diagnosis, treatment and follow-up. *Ann Oncol.* 2015;26(Suppl 5):v116-v125.
55. Kelly PN, Romero DL, Yang Y, et al. Selective interleukin-1 receptor-associated kinase 4 inhibitors for the treatment of autoimmune disorders and lymphoid malignancy. *J Exp Med.* 2015;212(13):2189-2201.
56. Takeuchi O, Akira S. Pattern recognition receptors and inflammation. *Cell.* 2010;140(6):805-820.

2016 127: 2732-2741
doi:10.1182/blood-2015-11-684183 originally published online April 5, 2016

B-cell–specific conditional expression of *Myd88*$^{p.L252P}$ leads to the development of diffuse large B-cell lymphoma in mice

Gero Knittel, Paul Liedgens, Darya Korovkina, Jens M. Seeger, Yussor Al-Baldawi, Mona Al-Maarri, Christian Fritz, Katerina Vlantis, Svetlana Bezhanova, Andreas H. Scheel, Olaf-Oliver Wolz, Maurice Reimann, Peter Möller, Cristina López, Matthias Schlesner, Philipp Lohneis, Alexander N. R. Weber, Lorenz Trümper, German International Cancer Genome Consortium Molecular Mechanisms in Malignant Lymphoma by Sequencing Project Consortium, Louis M. Staudt, Monika Ortmann, Manolis Pasparakis, Reiner Siebert, Clemens A. Schmitt, Andreas R. Klatt, F. Thomas Wunderlich, Stephan C. Schäfer, Thorsten Persigehl, Manuel Montesinos-Rongen, Margarete Odenthal, Reinhard Büttner, Lukas P. Frenzel, Hamid Kashkar and H. Christian Reinhardt

Blood (print ISSN 0006-4971, online ISSN 1528-0020), is published weekly by the American Society of Hematology, 2021 L St, NW, Suite 900, Washington DC 20036.

Supplemental Text

Supplemental Materials and Methods

Immunoblot

Cells were lysed (Cell Signaling lysis buffer supplemented with phosphatase inhibitor cocktail [Calbiochem]) and equivalent amounts of protein (60 µg in Laemmli buffer) were separated on 12.5% SDS-PAGE and blotted on PVDF membranes (Immobilon-P, Millipore, 0.45 µm). Membranes were stained with specific antibodies against MYD88 (Cell Signaling, D80F5) and β-actin (Sigma, A2228). Proteins were detected using the ECL Western Blotting Detection Kit (GE Healthcare).

Southern blot

Proper genomic integration of the *Myd88*-targeting vector was monitored using Southern blot analysis from BauI genomic DNA-digests to monitor the 5' integration event using a ~300 bp fragment from the genomic sequence upstream of exon 1 that lies outside the targeting construct as the 5' probe **(Fig. 1A)**. The probe was generated by PCR amplification followed by radiolabeling with ^{32}P-α-CTP using random priming. In the wildtype genomic *Myd88* sequence, the BauI digest gives rise to an 8.8 kb band, while correct 5' integration of the targeted allele gives rise to a 6 kb band due to the presence of a BauI site within the *Neo^R* cassette **(Fig. 1A)**. The 3' integration event was monitored by Southern blotting using a ~300 bp probe corresponding to the 3' flanking region outside the targeting construct (3' probe)**(Fig. 1A)**. The targeted allele gives rise to a 13.3 kb band, while the wildtype band runs at 11.2 kb **(Fig. 1A)**. Single integration of the targeting vector was verified using a probe that hybridizes with the *Neo^R* sequence (neo probe) on a KpnI genomic digest. The correct targeting event gives rise to a 6.8 kb band. No other bands were visible on the Southern blot, indicating a unique integration event **(Fig. 1A).**

Correct integration of the *Rosa26*-targeting vector was monitored using Southern blot analysis from EcoRI genomic DNA-digests to monitor the 5' integration event using a ~300 bp fragment from the genomic sequence upstream of exon 1 as the 5' probe **(Fig. S5C, S5D)**. The probe was

generated by PCR amplification followed by radiolabeling with ^{32}P-α-CTP using random priming. In the wildtype genomic *Rosa26* sequence, the EcoRI digest gives rise to a 16 kb band, while correct 5' integration of the targeted allele gives rise to a 7.1 kb band due to the presence of an EcoRI site within the *Neo^R* cassette **(Fig. S5C)**. Single integration of the targeting vector was verified using the neo probe on an EcoRI genomic digest. The correct targeting event gives rise to a 7.1 kb band. No other bands were visible on the Southern blot, indicating a unique integration event **(Fig. S5D).** For Southern blot analysis of VDJ-rearrangement, genomic DNA derived from primary and secondary lymphoid tissues was digested with EcoRI and transferred to a Hybond membrane after gel electrophoresis. The 250 bp probe JH4, derived from the VDJ plasmid via HindIII/NaeI digestions, was labeled with ^{32}P-α-CTP and results in a 6.2 kb band for germinal center configuration, while VDJ-rearranged alleles give bands of different sizes **(see Fig. S4B)**.

MR imaging

MR imaging was performed on a clinical 3.0T MRI system (Ingenia, Philips, the Netherlands) using a small rodent solenoid coil with a diameter of 40 mm and an implemented heating system to keep body temperature constant during MRI examination (Philips Research Europe, Hamburg, Germany). Animals were anesthetized by a 1.5 - 2.5% isoflurane inhalation. In order to depict anatomic details, high resolution transversal and coronal T2-weighted MR images of the abdomen were acquired with the following parameters: turbo spin echo (TSE) factor: 10, repetition time (TR): 2674 ms, echo time (TE): 65 ms, flip angle: 90°, slice thickness: 1.0 mm (without gap), voxel size (reconstructed): 0.16 x 0.16 x 1.0 mm, matrix: 256 x 256, field of view (FOV): 40 x 40 mm, and number of acquisition (NSA): 6, resulting in an acquisition time of 8:30 min for 25 slices. MR images were exported in DICOM format and analyzed using the research workstation Imalytics (Philips Innovative Technologies, Aachen, Germany). Semi-automatic segmentation of the spleen was performed and the volume of the spleen determined.

Tumor macrodissection and DNA extraction

Macrodissection of the tumor area was performed on six 10 µm sections of formalin-fixed and paraffin-embedded (FFPE) tissues. DNA was then

automatically extracted from the tumor areas using the Maxwell platform and Maxwell DNA FFPE isolation kit (Promega GmbH, Mannheim Germany) according to the manufacturer´s instructions.

NGS Library Construction by Multiplex PCR and deep sequencing

Targeted deep sequencing of FFPE extracted DNA was performed by a multiplex PCR covering the *ATM*, *BTK*, *CD79B*, *DDX3X*, *FBXW7*, *MAPK1*, *MYD88*, *NOTCH1*, *PIK3CA*, *PIK3CD*, *PTEN*, *PTPN6*, *SF3B1*, *TP53* and *XPO1* genes. First, DNA quality and quantity from FFPE lymphoma samples was assessed by qPCR as described previously [16,17]. 10 ng of amplifiable DNA was applied to multiplex PCR using the GeneRead *DNAseq* Panel PCR Kit *V2* (Qiagen Inc, Hilden GER) with primer sets that were previously established [16]. Amplicon purification was carried out by means of Agencourt® AMPure® XP magnetic beads (Beckman Coulter, Inc., Brea, CA, USA) on the robotic Biomek® FXP workstation (Beckman Coulter, Inc.). For further steps of library construction, the GeneRead DNA Library I Core Kit (Qiagen) was applied. PCR enriched DNA was adenylated and ligated to NEXTflex™ DNA barcodes (Bio Scientific, Austin, Texas, USA). After Agentcourt Ampure purification and size selection, barcoded DNA was further enriched by 10 PCR cycles using the NEXTflex™ primer mix (Bioo Scientific). The quality of amplicon libraries was evaluated by capillary electrophoresis using the QIAxcel Advanced System (Qiagen Inc) and 15 pM of the constructed library pools were finally applied to the MiSeq (Illumina, Inc., San Diego, Ca, USA) using the v2 chemistry as recommended by the manufacturer. Fastq files were generated by the MiSeq Reporter Software (Illumina, Inc.) and analyzed by the CLC Genomics Workbench program (Qiagen Inc). The experiments involving primary human material have been approved by the internal review board in the framework of the BioMaSOTA (Biologische Material Sammlung zur Optimierung Therapeutischer Ansätze) program.

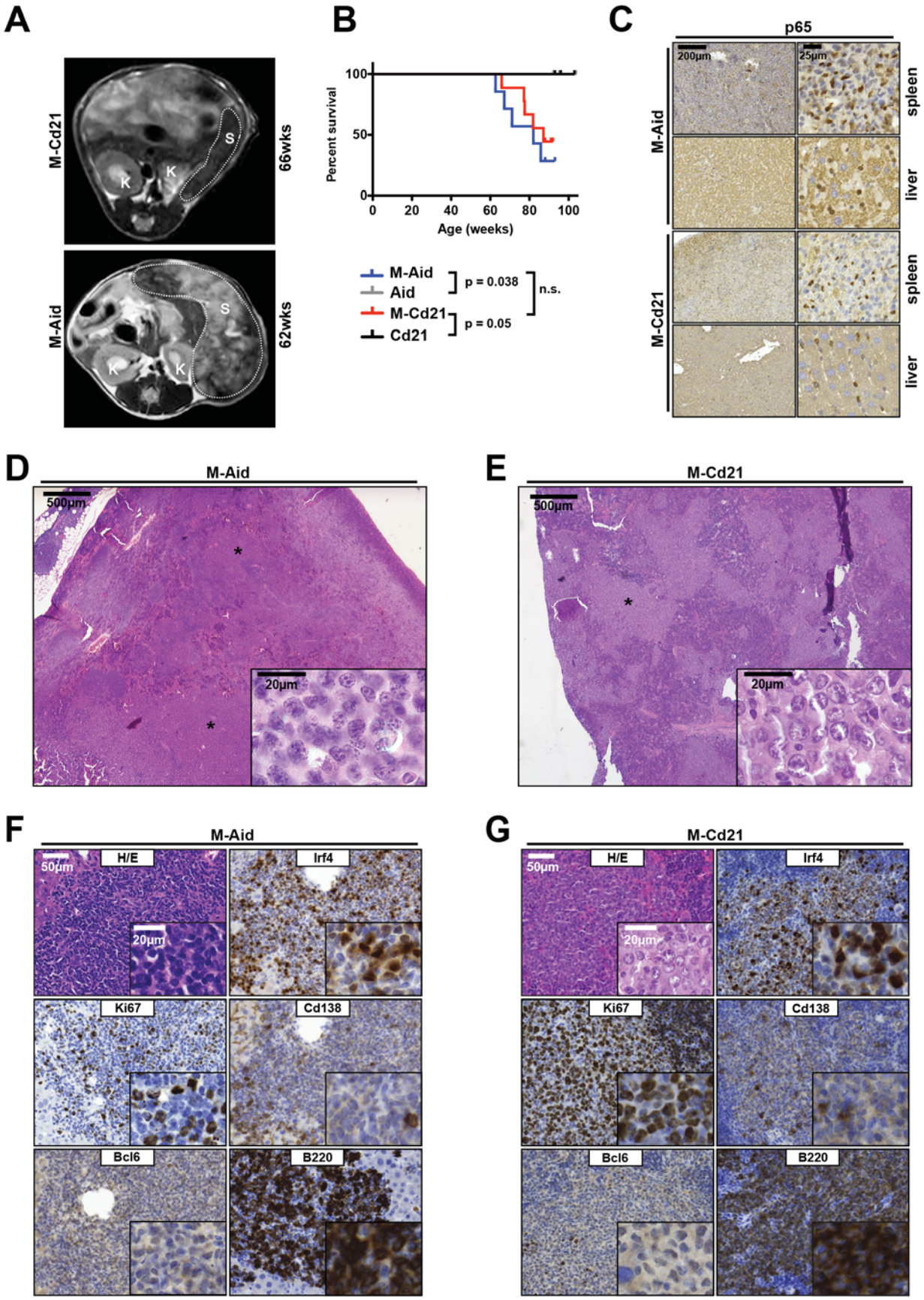

Supplemental Figure 1 - Activation of *Myd88*$^{p.L252P}$ by Aid-Cre or Cd21-Cre drives lympho-proliferation and lymphomagenesis, *in vivo*.

(A) MR imaging at the indicated times revealed the occurrence of splenomegaly in M-Aid and M-Cd21 mice (S, spleen; K, kidney).

(B) B cell-specific expression of *Myd88*$^{p.L252P}$ substantially reduces overall survival, *in vivo*. The overall survival of Aid, M-Aid, Cd21 and M-Cd21 mice is illustrated in Kaplan Meier format. M-Aid and M-Cd21 mice display a significantly reduced survival, compared to the respective controls.

(C) The infiltrates in M-Aid and M-Cd21 mice display nuclear p65 staining, indicating NF-κB activation.

(D) and **(E).** M-Aid and M-Cd21 mice develop lympho-proliferative disease and occasional lymphoma, resulting in a disruption of the splenic architecture. Representative H/E stainings of spleens of M-Aid and M-Cd21 animals are shown. Asterisks mark areas of infiltrates consisting of a homogeneous large cell population with blastoid appearance. These areas are also displayed in a higher magnification in the insets (bottom right).

In **(F)** and **(G)**, the immunophenotypes of M-Aid and M-Cd21 animals are shown. Cells in areas of homogeneous, blastoid infiltrates are B220- and Irf4-positive, but stain negative for Cd138 and Bcl6.

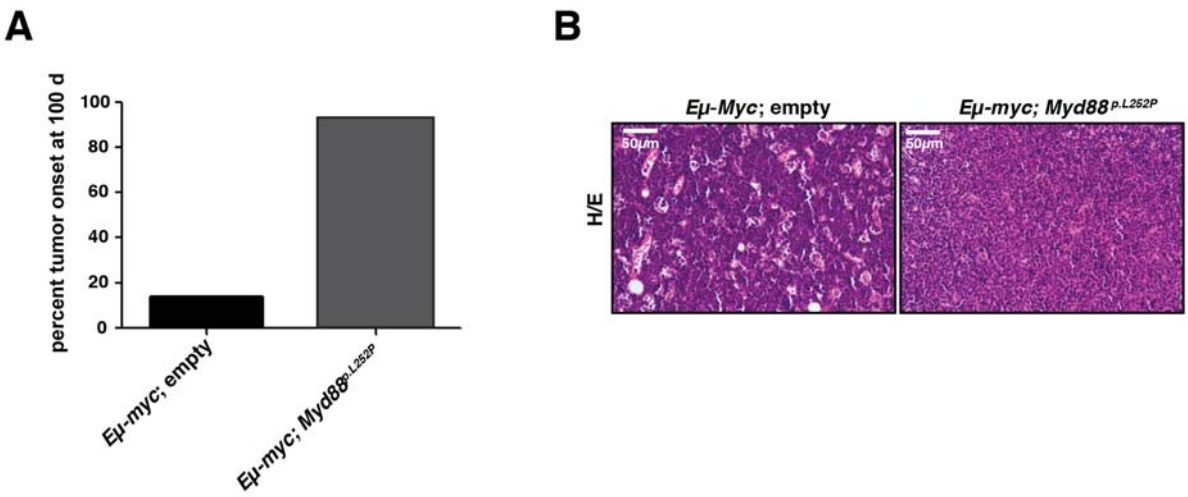

Supplemental Figure 2 – *Myd88*$^{p.L252P}$ expression accelerates onset of *Eμ:Myc*-driven B cell lymphomas.

A) The percentage of lethally irradiated mice with palpable lymphadenopathy at day 100 post transplantation with *Eμ:Myc* transgenic fetal liver cells stably transduced with either empty vector, or *Myd88*$^{p.L252P}$ is shown.

B) H/E stainings of overt lymphomas manifested in lethally-irradiated recipient mice that were transplanted with *Eμ:Myc* transgenic fetal liver cells stably transduced with either empty vector, or *Myd88*$^{p.L252P}$.

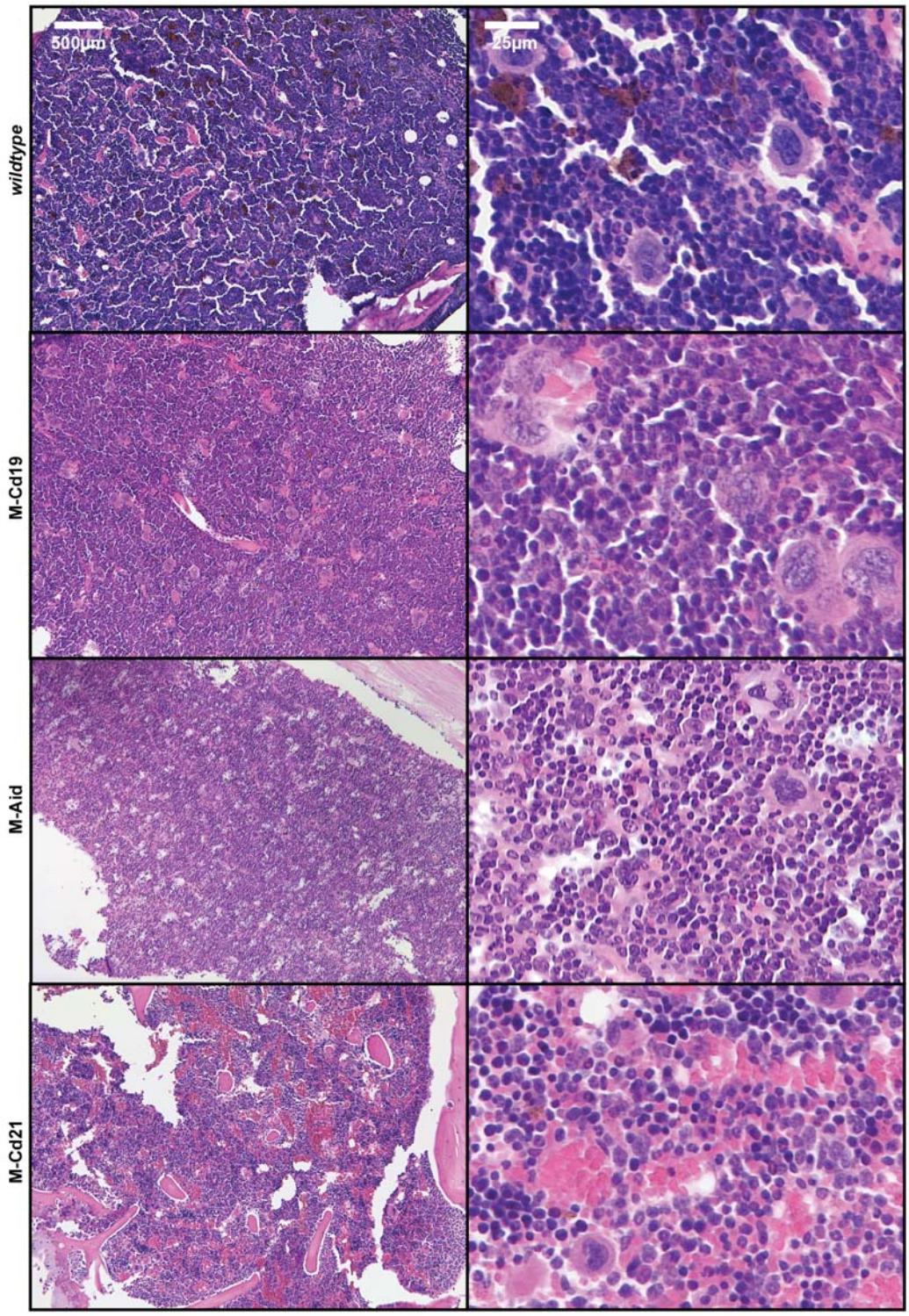

Supplemental Figure 3 – M-Cd19, M-Cd21 and M-Aid mice do not display bone marrow infiltration.

Histological examination of the bone marrow (n = 3 per genotype) did not reveal any signs of infiltration of the bone marrow by a lymphoid or lympho-blastoid population.

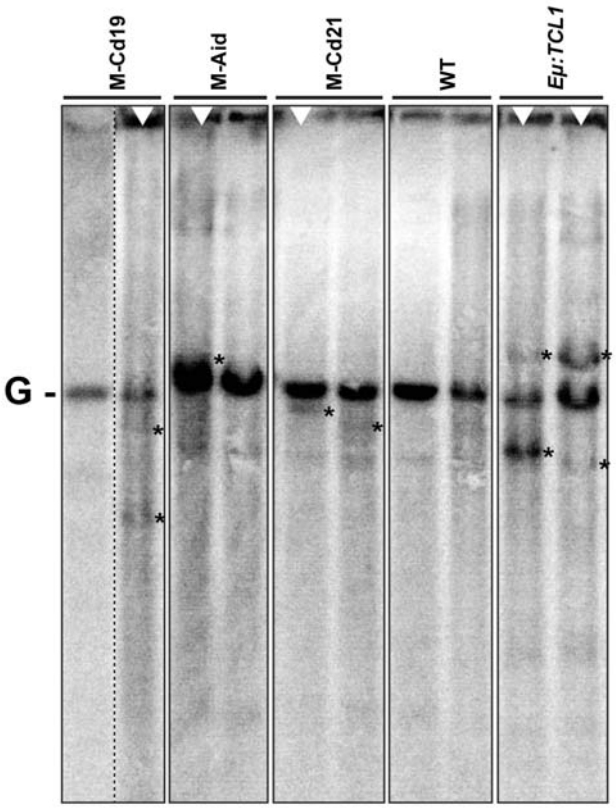

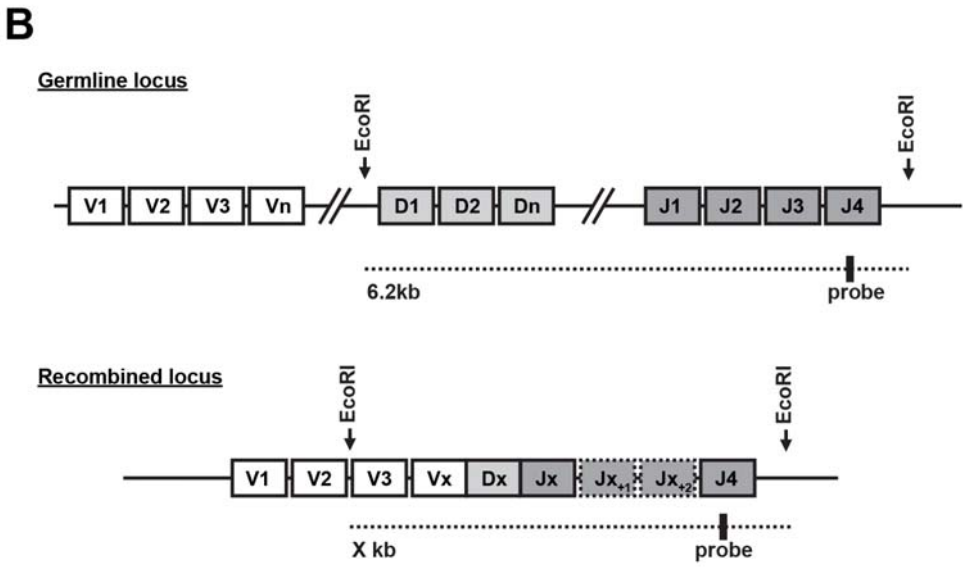

Supplemental Figure 4 - A subset of M-Cd19, M-Aid and M-Cd21 shows clonal populations in VDJ-rearrangement analysis by Southern blot.

(A) Clonal VDJ rearrangement of M-Cd19, M-Aid and M-Cd21 animals was analyzed. The germline configuration is present also in the WT controls and depicted as 'G'. Asterisks indicate clonal rearrangements. Samples of animals with lymphoma detected by histological analyses are marked with a white triangle (top). **(B)** Schematic illustration of the southern blot strategy. The radioactively labeled probe

hybridizes within the J4 region. The size of the labeled EcoRI fragment depends on the selectd V-, D- and J segments.

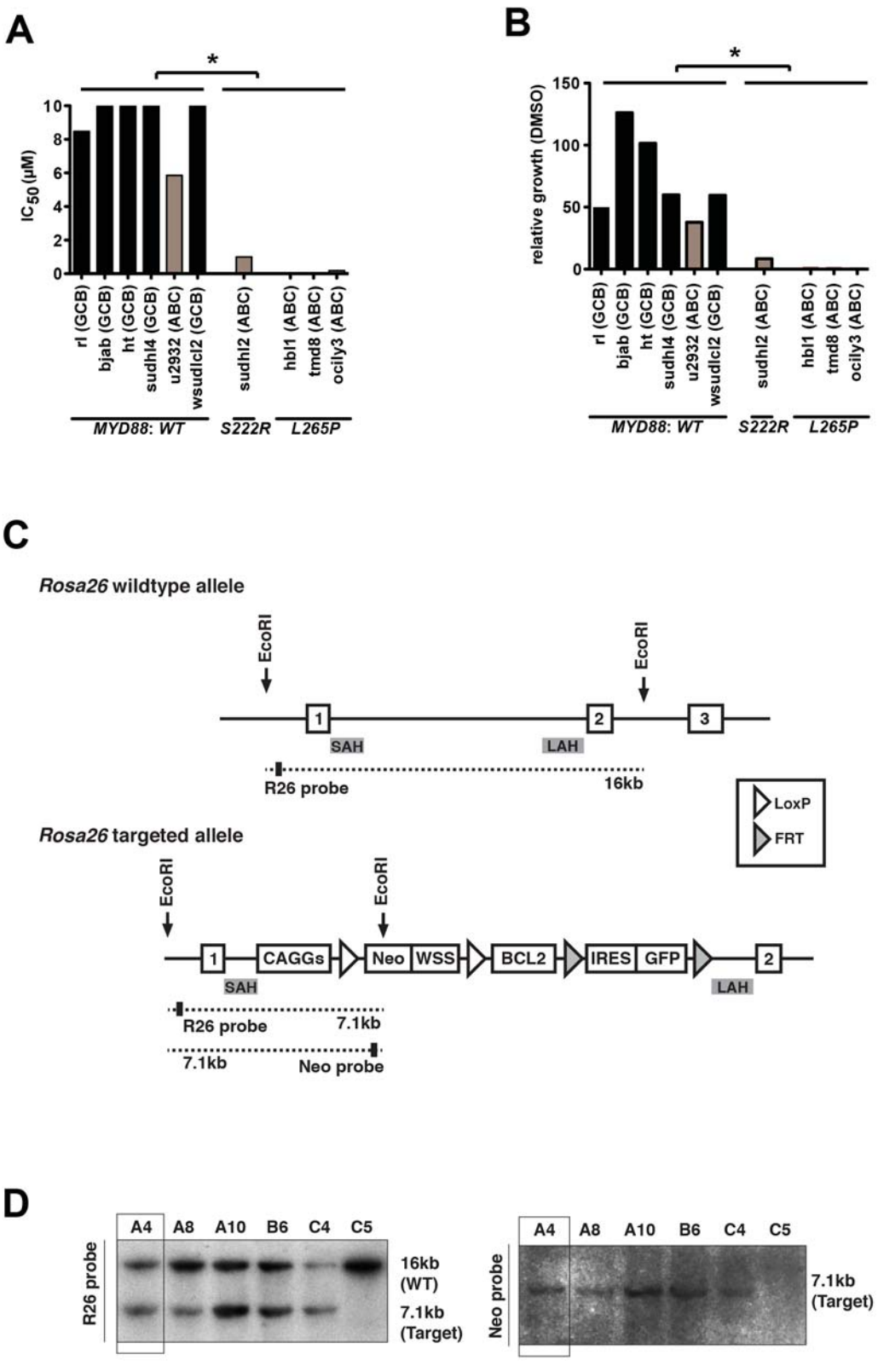

Supplemental Figure 5 - *MYD88*-mutant human DLBCL cell lines display sensitivity towards BCL-2/BCL-X_L-inhibition and construction of a conditional *Rosa26*$^{LSL.BCL2.IRES.GFP}$ allele.

Pharmacological profiling revealed that *MYD88*-mutant DLBCL cell lines show significantly increased sensitivity towards ABT-263-mediated BCL2/BCL-X_L inhibition,

compared with *MYD88 wildtype* DLBCL cell lines. Sensitivity data derived from [19] were assessed by half-maximum inhibitory concentration IC_{50} **(A)** and relative growth normalized to DMSO **(B)**. Significance was tested using Mann-Whitney U test. * indicates $p < 0.05$.

(C) Targeting of the *Rosa26* locus in *C57BL/6N* BRUCE4 ES cells. The endogenous *Rosa26* locus was targeted with the linearized vector described in the Materials and Methods section. The *Rosa26* allele before (top panel) and following homology-directed gene targeting (middle panel) is schematically depicted. The Southern blots of EcoRI-digested genomic DNA probed with a 5' and a Neo probe, respectively, are shown in **(D)**. Positions of restriction sites and probes are shown in **(C)**. SAH, short arm of homology; LAH, long arm of homology.

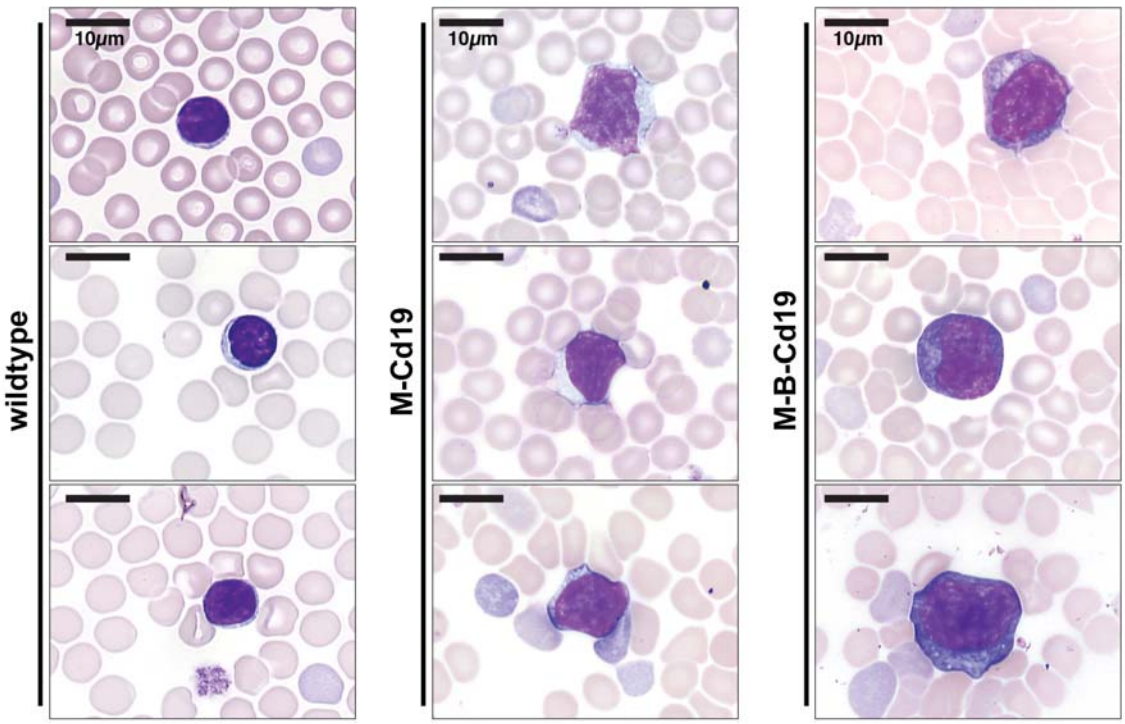

Supplemental Figure 6 – M-B-Cd19 mice develop leukemic effusion.

Representative blood smears of *C57BL/6 wildtype*, M-Cd19 and M-B-Cd19 mice at the time of death are shown. While normal lymphocytes are detectable in *C57BL/6 wildtype* mice (left panel), the majority of lymphocytes in M-Cd19 blood smears appeared to be activated (middle panel). Morphological analysis of blood smears from M-B-Cd19 mice revealed the presence of lymphoma cells in the peripheral blood (right panel).

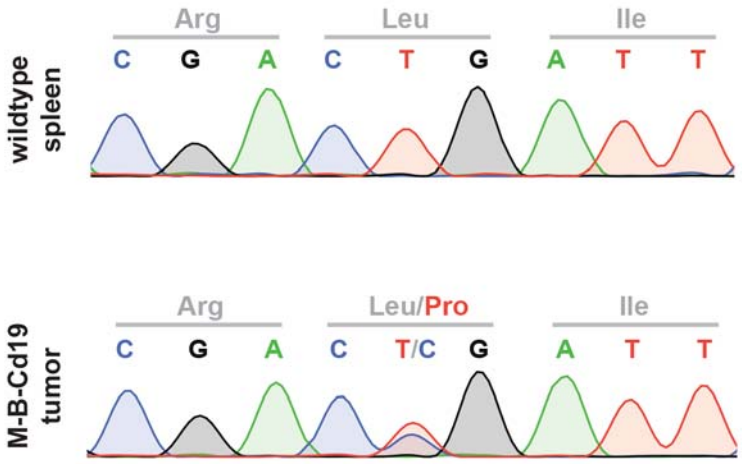

Supplemental Figure 7 - Lymphomas from M-B-Cd19 animals express *Myd88*$^{p.L252P}$.

RNA was extracted from fresh-frozen tumors isolated from M-B-Cd19 animals, reverse-transcribed and sequenced. Mutant cDNA was only detected in tumors, but not in *wildtype* control.

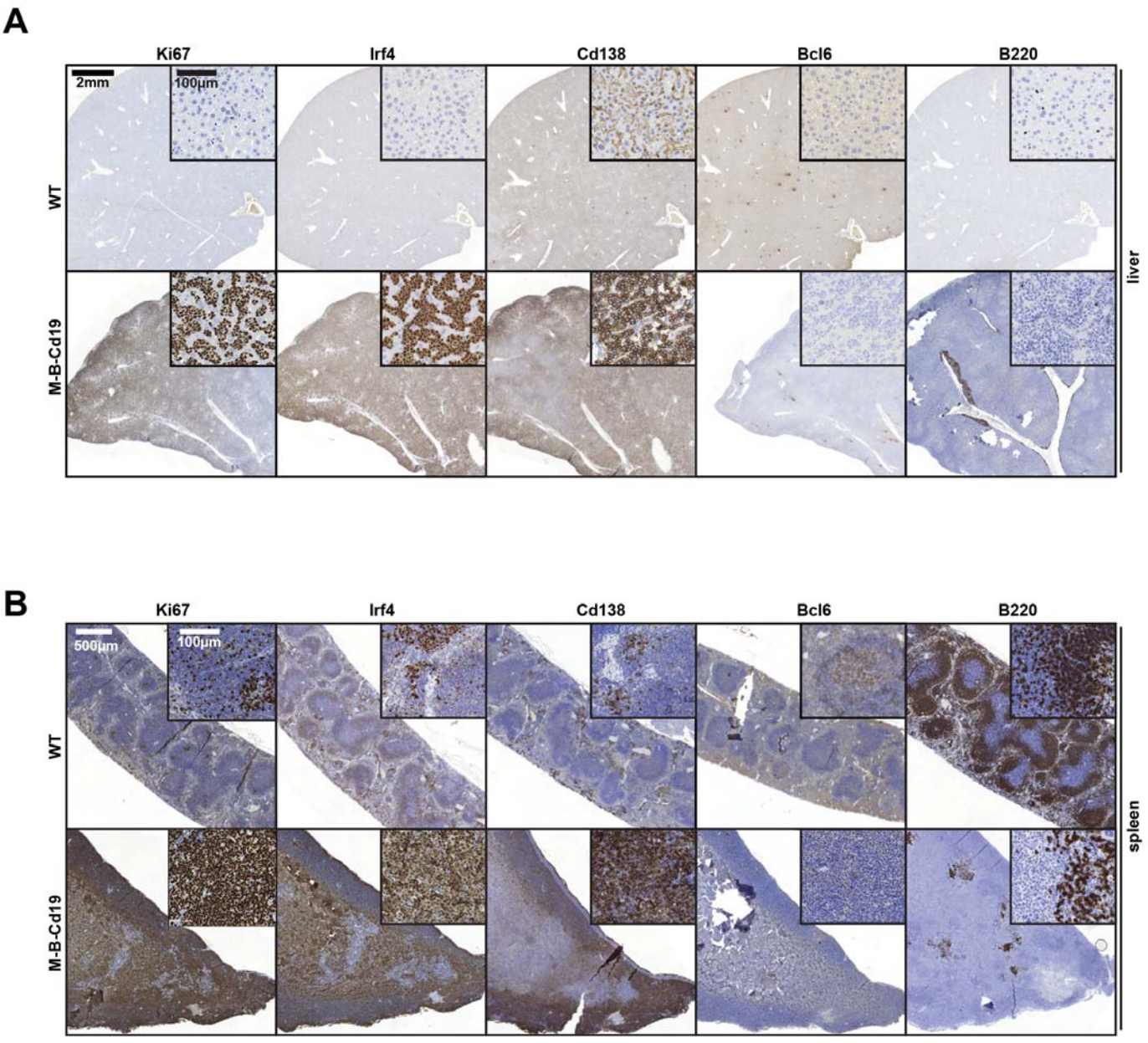

Supplemental Figure 8 - Immunohistochemical stainings of M-B-Cd19 tumors. Livers **(A)** and spleens **(B)** of M-B-Cd19 mice were infiltrated with a homogeneous cell population that with a $B220^{-}$ $Bcl6^{-}$ $Cd138^{+}$ $Irf4^{+}$ staining pattern with a high Ki67 index.

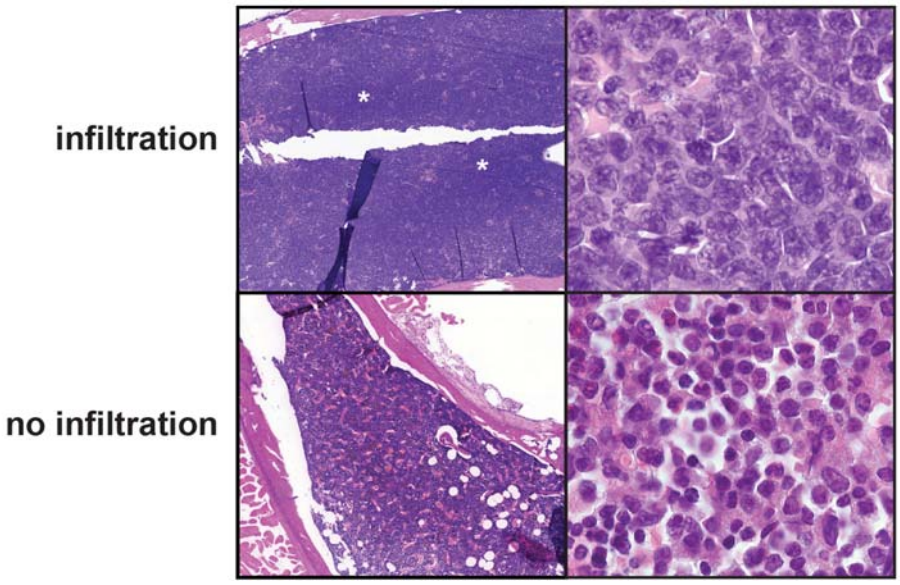

Supplemental Figure 9 - Bone marrow involvement is a rare event in M-B-Cd19 animals.

Histological examination of the bone marrow of 4 distinct M-B-Cd19 mice revealed locally restricted lymphoma infiltrate in one animal.

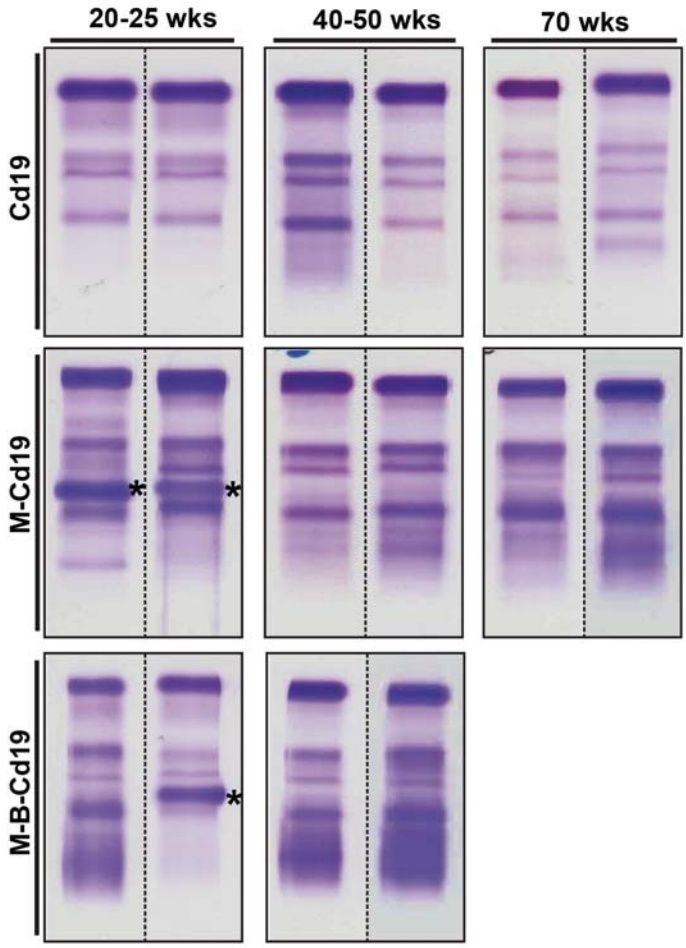

Supplemental Figure 10 - Polyclonal gammopathy in M-B-Cd19 mice.

Serum of Cd19, M-Cd19 and M-B-Cd19 mice of different ages was analyzed by serum protein gel electrophoresis. M-B-Cd19 animals develop polyclonal gammopathy. Polyclonal gammopathy was also observed in M-Cd19 animals, albeit with lower frequency and to a more moderate degree. Asterisks mark contaminating haemoglobin bands, a technical artifact of serum preparation.

Knittel et al., Supplementary Table 1

sample name	gene	AA mutation	frequency	forward/ reverse balance
2	ATM	I1407T	14.82	0.50
4	NOTCH1	P1377S	46.98	0.49
5	NOTCH1	P1386S	6.24	0.08
5	ATM	Y2019C	13.79	0.50
5	CD79B	Y196C	31.56	0.26
5	NOTCH1	V726I	46.77	0.50
5	MYD88	S251N	54.10	0.50
5	NOTCH1	P1377S	55.69	0.49
6	ATM	Y2019C	14.29	0.50
7	TP53	E258K	43.25	0.47
7	NOTCH1	R1279H	47.66	0.47
9	FBXW7	D440N	6.45	0.50
10	CD79B	Y196H	31.15	0.23
11	DDX3X	R528C	5.88	0.50
12	ATM	Y2019C	10.00	0.50
14	MYD88	L265P	37.17	0.50
17	PTEN	C105F	5.13	0.50
17	TP53	Q317*	7.41	0.50
17	TP53	Q331*	7.50	0.50
17	TP53	Y327*	7.55	0.50
19	ATM	Y2019C	18.18	0.50
21	TP53	A161D	8.02	0.49
21	NOTCH1	Q2406*	12.98	0.49
21	ATM	I1407T	14.51	0.49
21	TP53	I255S	49.94	0.49
22	PTEN	L112V	6.00	0.40
22	PTEN	I101T	6.25	0.40
22	PTEN	C105F	6.52	0.40
22	CD79B	Y196H	32.88	0.25
23	PTEN	H93Q	7.08	0.14
24	ATM	Y2019C	6.06	0.50
24	TP53	M246I	53.09	0.50
26	MYD88	L265P	13.22	0.50
26	CD79B	Y196F	35.09	0.25
27	TP53	R213*	29.71	0.50
28	MYD88	L265P	29.39	0.50
28	CD79B	Y196S	38.68	0.21
29	SF3B1	L25P	8.57	0.50
29	TP53	A86fs	90.07	0.50
31	ATM	P884S	7.52	0.50
32	TP53	R248Q	45.50	0.50
32	CD79B	Y196C	94.75	0.20
34	MYD88	S219C	5.00	0.50
34	ATM	Y2019C	7.14	0.50
35	MYD88	S251N	38.30	0.49
36	CD79B	Y196C	77.27	0.14
38	ATM	Q2522H	50.00	0.26
39	ATM	Y2019C	8.70	0.50
39	NOTCH1	R1279H	22.80	0.48
39	MYD88	L265P	32.74	0.50
39	CD79B	Y196N	38.98	0.22
41	DDX3X	T532M	28.29	0.50
41	MYD88	S219C	33.04	0.50
42	ATM	Y2019C	10.00	0.50
43	TP53	D207G	24.53	0.49
43	TP53	V123G	45.06	0.49
45	MYD88	L265P	55.70	0.50
47	TP53	R282W	49.58	0.49

47	CD79B	Y196C	68.06	0.26
48	TP53	L45P	15.38	0.50
48	TP53	Q38*	15.38	0.50
48	TP53	E258K	49.49	0.47
49	ATM	R2443*	5.56	0.33
49	CD79B	Y196H	26.38	0.26
50	MYD88	D148Y	17.12	0.50
50	NOTCH1	P2227L	49.07	0.48
50	ATM	P1054R	54.22	0.09
51	PIK3CA	R524K	5.05	0.48
51	CD79B	Y196S	38.59	0.28
51	CD79B	Y196S	41.34	0.29
52	TP53	Y163C	11.04	0.50
53	ATM	I352T	7.14	0.50

Full list of members of the ICGC MMML-Seq

Coordination (C1): Gesine Richter[1], Reiner Siebert[1], Susanne Wagner[1], Andrea Haake[1], Julia Richter[1]
Data Center (C2): Roland Eils[2,3], Chris Lawerenz[2], Sylwester Radomski[2], Ingrid Scholz[2]
Clinical Centers (WP1): Christoph Borst[4], Birgit Burkhardt[5,6], Alexander Claviez[7], Martin Dreyling[8], Sonja Eberth[9], Hermann Einsele[10], Norbert Frickhofen[11], Siegfried Haas[4], Martin-Leo Hansmann[12], Dennis Karsch[13], Michael Kneba[13], Jasmin Lisfeld[6], Luisa Mantovani-Löffler[14], Marius Rohde[5], Christina Stadler[9], Peter Staib[15], Stephan Stilgenbauer[16], German Ott[17], Lorenz Trümper[9] , Thorsen Zenz[35]
Normal Cells (WPN): Martin-Leo Hansmann[12], Dieter Kube[9], Ralf Küppers[18], Marc Weniger[18]
Pathology and Analyte Preparation (WP2-3): Siegfried Haas[4], Michael Hummel[19], Wolfram Klapper[20], Ulrike Kostezka[21], Dido Lenze[19], Peter Möller[22], Andreas Rosenwald[23], Monika Szczepanowski[20]
Sequencing and genomics (WP4-7): Ole Ammerpohl[1], Sietse Aukema[1], Vera Binder[24], Arndt Borkhardt[24], Andrea Haake[1], Kebria Hezaveh[24], Jessica Hoell[24]; Ellen Leich[23], Peter Lichter[2], Christina Lopez[1], Inga Nagel[1], Jordan Pischimariov[23], Bernhard Radlwimmer[2], Julia Richter[1], Philip Rosenstiel[25], Andreas Rosenwald[23], Markus Schilhabel[25], Stefan Schreiber[26], Inga Vater[1], Rabea Wagner[1], Reiner Siebert[1]
Bioinformatics (WP8-9): Stephan H. Bernhart[27-29], Hans Binder[28], Benedikt Brors[2], Gero Doose[27-29], Jürgen Eils[2], Roland Eils[2,3], Steve Hoffmann[27-29], Lydia Hopp[28], Helene Kretzmer[27-29], Markus Kreuz[30], Jan Korbel[31], David Langenberger[27-29], Markus Loeffler[30], Sylwester Radomski[2], Maciej Rosolowski[30], Matthias Schlesner[2] , Peter F. Stadler[27-29,32-34], Stefanie Sungalee[31]

[1]Institute of Human Genetics, University Hospital Schleswig-Holstein Campus Kiel/ Christian-Albrechts University Kiel, Kiel, Germany;
[2]German Cancer Research Center (DKFZ), Division Theoretical Bioinformatics, Heidelberg, Germany;
[3]Department for Bioinformatics and Functional Genomics, Institute for Pharmacy and Molecular Biotechnology and Bioquant, University of Heidelberg, Heidelberg, Germany;
[4]Friedrich-Ebert Hospital Neumünster, Clinics for Hematology, Oncology and Nephrology, Neumünster, Germany;
[5]Department of Pediatric Hematology and Oncology, University Hospital Münster, Münster, Germany;

[6]Department of Pediatric Hematology and Oncology University Hospital Giessen, Giessen, Germany;
[7]Department of Pediatrics, University Hospital Schleswig-Holstein, Campus Kiel, Germany;
[8]Department of Medicine III - Campus Grosshadern, University Hospital Munich, Munich, Germany;
[9]Department of Hematology and Oncology, Georg-August-University of Göttingen, Göttingen, Germany;
[10]University Hospital Würzburg, Department of Medicine and Poliklinik II, University of Würzburg, Würzburg, Germany;
[11]Department of Medicine III, Hematology and Oncology, Dr. Horst-Schmidt-Kliniken of Wiesbaden, Wiesbaden, Germany;
[12]Senckenberg Institute of Pathology, University of Frankfurt Medical School, Frankfurt am Main, Germany;
[13]Department of Internal Medicine II: Hematology and Oncology, University Medical Centre, Campus Kiel, Kiel, Germany;
[14]Hospital of Internal Medicine II, Hematology and Oncology, St-Georg Hospital Leipzig, Leipzig, Germany;
[15]Univesity Hospital Aachen, St.-Antonius Hospital, Department of Oncology, Hematology and stem cell transplantation, University of Aachen, Aachen, Germany;
[16]Department of Internal Medicine III, University of Ulm, Ulm, Germany;
[17]Robert-Bosch Hospital Stuttgart, Department of Pathology, Stuttgart, Germany;
[18]Institute of Cell Biology (Cancer Research), University of Duisburg-Essen, Essen, Germany;
[19]Institute of Pathology, Charité – University Medicine Berlin, Berlin, Germany;
[20]Hematopathology Section, University Hospital Schleswig-Holstein Campus Kiel/ Christian-Albrechts University Kiel, Kiel, Germany;
[21]Comprehensive Cancer Center Ulm (CCCU), University Hospital Ulm, Ulm, Germany;
[22]Institute of Pathology, Medical Faculty of the Ulm University, Ulm, Germany;
[23]Institute of Pathology, University of Würzburg, Würzburg, Germany;
[24]Department of Pediatric Oncology, Hematology and Clinical Immunology, Heinrich-Heine-University, Düsseldorf, Germany;
[25]Institute of Clinical Molecular Biology, University Hospital Schleswig-Holstein Campus Kiel/ Christian-Albrechts University Kiel, Kiel, Germany;
[26]Department of General Internal Medicine, University Hospital Schleswig-Holstein Campus Kiel/ Christian-Albrechts University Kiel, Kiel, Germany;
[27]Transcriptome Bioinformatics Group, LIFE Research Center for Civilization Diseases, Leipzig, Germany;
[28]Interdisciplinary Center for Bioinformatics, University of Leipzig, Leipzig, Germany;
[29]Bioinformatics Group, Department of Computer, University of Leipzig, Leipzig, Germany
[30]Institute for Medical Informatics Statistics and Epidemiology, Leipzig, Germany;
[31]EMBL Heidelberg, Genome Biology, Heidelberg, Germany;
[32]RNomics Group, Fraunhofer Institute for Cell Therapy and Immunology IZI, Leipzig, Germany
[33]Santa Fe Institute, Santa Fe, New Mexico, United States of America
[34]Max-Planck-Institute for Mathematics in Sciences, Leipzig, Germany
[35]Department of Medicine V, University of Heidelberg, Heidelberg, Germany